

NATIONAL TRANSPORTATION SAFETY BOARD

Office of Research and Engineering
Materials Laboratory Division
Washington, D.C. 20594



May 9, 2011

MATERIALS LABORATORY STUDY REPORT

Report No. 11-058

A. ACCIDENT INFORMATION

Place : San Bruno, California
Date : September 9, 2010
Vehicle : Natural Gas Transmission Pipeline
NTSB No. : DCA10MP008
Investigator : Ravi Chhatre

B. TOPICS ADDRESSED

Finite element modeling to examine stresses in sections of pipe.

C. DETAILS OF THE STUDY

Two finite element models were constructed to examine the stresses in sections of pipe with differing longitudinal seam welds. Model 1 was based on the idealized geometry of a section of pipe with a double submerged arc weld (DSAW) seam having no defects [see figure 44 of Reference 1]. Model 2 was based on the observed geometry of the short section of pipe having a seam weld with incomplete penetration where the fracture was identified to have originated [Pup 1 in figure 45 of Reference 1].

The finite element modeling was carried out using ABAQUS Standard 6.10, which employs an implicit solution methodology. The finite element models were two-dimensional, using an assumption of plane strain. All dimensions are in inches. Nonlinear materials properties were included in the models, and nonlinear geometric effects were permitted in the solution. Loads were applied quasistatically. No material softening or crack propagation was considered for this study.

1. Geometry

a. Model 1 - Nominal pipe with DSAW seam with no defects

The overall geometry is shown in figure 1, with the welded seam placed at the top of the cylindrical section of pipe. The outer diameter of the pipe was input as 30.000 inches, and the inner diameter was input as 29.250 inches, with a resulting thickness of 0.375 inch. The inner and outer weld beads were modeled as having an elliptical shape, with a major axis of 1.000 inch and a minor axis of 0.750 inch. The center of the ellipse for the outer weld bead was placed at a radius of 14.740 inch, and the center of the ellipse for the inner weld bead was placed at a radius of 14.885 inch. The resulting weld beads extended laterally approximately 0.72 inch along the pipe, with

a height of 0.115 inch relative to the wall of the pipe. The four corners where the weld beads intersected the circular pipe walls were each given a fillet radius of 0.004 inch.

b. Model 2 - Pipe with seam weld with incomplete penetration

The overall geometry is shown in figure 2, with the welded seam placed at the top of the cylindrical section of pipe. The outer diameter of the pipe was input as 30.000 inches, and the inner diameter was input as 29.260 inches, with a resulting thickness of 0.370 inch, based on the measured wall thickness of Pup 1 in Reference 1. The details of the geometry of the seam will be described by coordinates referenced to the center of the pipe, with dimensions in inches. Figures 3, 4 and 5 show the geometry at the seam, with the coordinates of the labeled points indicated in table 1. On either side of the weld, the walls of the pipe were straight, and did not conform to the overall circular shape of the pipe. These two straight sections were asymmetric, and they intersected with an offset at the inner surface of the pipe wall. At the outer surface, the pipe wall and weld bead were ground down to form a smooth arc, which was modeled as a circle with a radius of 6.5 inches centered at (0.067, 8.568). The uncracked ligament was taken to be 0.160 inch, and the end of the unwelded notch was modeled as a semicircle with radius of 0.004 inch centered at (0, 14.904), based on the measured width of the notch in figure 48 of Reference 1.

Table 1. Control points for the geometry of the pipe seam having a weld with incomplete penetration, as shown in figures 3 through 5.

Control point	X position (inches)	Y position (inches)
A	-1.732	14.527
B	-0.004	14.733
C	-0.004	14.904
D	0.000	14.904
E	0.004	14.904
F	0.004	14.763
G	1.960	14.498
H	-1.776	14.895
I	-0.703	15.023
J	0.938	15.010
K	2.010	14.865

c. Material properties

An elastic/plastic constitutive law was used for the steel in the pipe models. Young's modulus for steel was taken as 29,000 ksi, and Poisson's ratio was taken as 0.3. Representative nonlinear constitutive behavior for pipeline steel was input to the models. Tensile tests of a weld being impractical, the material properties were adapted from the results of a uniaxial tensile test performed on a section of pipe from the same

line as the rupture, but some 700 feet upstream [Reference 2]. The curve was revised to match a 0.5 % strain offset yield stress of 42 ksi, based on a regression fit of microhardness data [see figure 26 of Reference 3], and the ultimate engineering tensile stress (at the onset of necking) was set to be 73 ksi, based on a regression fit of tensile strength data [also in figure 26 of Reference 3]. The measured data are shown in figure 6, and the data used as input to the model are shown in figure 7. Note that the stress/strain behavior does not exhibit a sharp yield point, so that nonlinearity begins at a stress that is approximately half of the 0.5 % strain offset yield stress. The data in figure 6 represent the engineering stress and strain based on the undeformed geometry of the test sample. For input to the finite element model, the engineering strain ε_n and engineering stress σ_n were converted to true strain ε and true stress σ , with

$$\varepsilon = \ln(1 + \varepsilon_n) \quad (1)$$

$$\sigma = \sigma_n (1 + \varepsilon_n) \quad (2)$$

[Reference 4]. The plastic strain ε_p was calculated by subtracting the elastic strain from the true strain, with

$$\varepsilon_p = \varepsilon - \frac{\sigma}{E} \quad (3)$$

where E is Young's modulus. The nonlinear behavior was input to the model as true stress versus plastic strain pairs, as shown in table 2. The plastic strain is zero at the onset of nonlinearity. Beyond the last stress/strain pair in the table, the behavior is assumed to be perfectly plastic, so that the stress remains constant for strains beyond the final strain value in the table.

True Stress (ksi)	Plastic Strain (%)
20.3	0.0
25.0	0.0190
30.3	0.0564
35.0	0.125
40.3	0.277
42.2	0.353
47.3	0.584
54.3	1.27
61.1	2.41
67.3	3.98
73.5	6.10
79.5	8.98
81.8	11.1
83.2	12.9
84.0	13.7

d. Loads and boundary conditions

For both models, the only load applied was pressure at the inner surface of the pipe, with zero pressure applied at the exterior of the pipe. For Model 2, the pressure was also applied on the inner surface of the notch where the weld metal did not penetrate the joint. The pressures were applied to three target values in three steps, first to a pressure of 350 psi, then to a pressure of 375 psi, and finally to a pressure of 400 psi. For Model 2, the first step to the pressure of 350 psi was subdivided into 10 sub-steps to track the onset and magnitude of nonlinear behavior.

As noted above, the weld was located at the top of the pipe in each model. In order to prevent rigid-body motions, the pipe was held fixed (no displacement or rotation) at a single node at the bottom of the pipe, opposite the weld in each model.

e. Mesh

The models were meshed with linear plane strain elements, using primarily quadrilateral elements, but with some triangular elements allowed to facilitate mesh-size transitions. The element sizes were biased to be smaller near the areas of stress concentrations, which occur at the corners of the weld bead for Model 1, and at the notch formed by the lack of weld metal in the seam for Model 2. Figures 8 and 9 indicate the mesh geometry near the stress concentrations for the two models. For Model 1, the smallest mesh dimension was approximately 0.0002 inch, and the mesh included 108,423 nodes, with 104,720 reduced integration quadrilateral elements (CPE4R) and 2,195 triangular elements (CPE3); away from the seam, the model had 8 quadrilateral elements through the thickness of the pipe wall. For Model 2, the smallest mesh dimension was approximately 0.0001 inch and the mesh included 201,495 nodes, with 197,404 reduced integration quadrilateral elements (CPE4R) and 3,470 triangular elements (CPE3); away from the seam, the model had 7 quadrilateral elements through the thickness of the pipe wall. No formal mesh convergence study was performed for either model.

f. Output

Figures 10 through 21 show contours of the Mises stress in the models near the seams at pressure levels of 350 psi, 375 psi and 400 psi. The Mises stress governs the development of the plastic strain, and for Model 2, the Mises stress reaches the maximum stress of 84.0 ksi input to the model in table 2. The contour levels are in psi and are the same for figures 10 through 21. The figures are presented in pairs, with the bottom figure being a magnified view of the contours at a stress concentration. The figures from the two models are shown at the same scales, with the bottom figures being magnified by 6 times relative to the top figures. Table 3 presents the peak values of the Mises stress for the model of the pipe having a welded seam with no defect, and table 4 presents the peak values of the Mises stress for the model of the pipe having a seam with incomplete weld penetration.

Figures 22 through 33 show contours of the maximum principal stress in the models near the seams at pressure levels of 350 psi, 375 psi and 400 psi. The maximum principal stress contours indicate the magnitude of the maximum tensile stress at any point, but do not indicate orientation. Again, the contour levels are in psi and are the same for figures 22 through 33, and the figures are presented in pairs, with the bottom figure being a magnified view of the contours at a stress concentration. The figures from the two models are shown at the same scales, with the bottom figures being magnified by 6 times relative to the top figures. Table 3 also presents the peak values of the maximum principal stress for the model of the pipe having a welded seam with no defect, and table 4 presents the peak values of the maximum principal stress for the model of the pipe having a seam with incomplete weld penetration.

Table 3. Peak values of the Mises stress and the maximum principal stress in the model of the pipe having a welded seam with no defect.

Pressure (psi)	Mises Stress (ksi)	Maximum Principal Stress (ksi)
350	34.1	39.5
375	35.2	41.0
400	36.1	42.1

Table 4. Peak values of the Mises stress and the maximum principal stress in the model of the pipe having a seam with incomplete weld penetration.

Pressure (psi)	Mises Stress (ksi)	Maximum Principal Stress (ksi)
35	43.2	53.4
70	54.8	74.6
105	62.7	90.2
140	70.3	103.8
175	77.7	114.5
210	82.7	123.3
245	84.0	130.8
280	84.0	137.0
315	84.0	142.7
350	84.0	147.2
375	84.0	150.1
400	84.0	152.8

The elastic stresses in the pipe models away from any stress concentrations can be compared with analytical equations for the stresses in a cylindrical shell under

internal pressure. These comparisons are shown for both pipe models in figures 34 through 39, for a pressure of 400 psi. The data from the models were taken from elements diametrically opposite the seams in each case, in order to make the closest comparison to the equations, which are derived for perfect cylinders with no seams. The stress components shown in the figures were taken from the central integration points of a radial row of elements. The circumferential stress σ_θ , radial stress σ_r and axial stress σ_z (assuming plane strain conditions) are given by

$$\sigma_\theta = \frac{a^2 p}{b^2 - a^2} \left(1 + \frac{b^2}{r^2} \right) \quad (4)$$

$$\sigma_r = \frac{a^2 p}{b^2 - a^2} \left(1 - \frac{b^2}{r^2} \right) \quad (5)$$

$$\sigma_z = \nu(\sigma_r + \sigma_\theta) = 2\nu \frac{a^2 p}{b^2 - a^2} \quad (6)$$

where p is the internal pressure, ν is Poisson's ratio, a is the inner radius of the pipe and b is the outer radius of the pipe [Reference 5]. Note that the axial stress in equation (6) is constant through the thickness.

As an alternative, the average circumferential stress σ_θ in the pipe can be computed as

$$\sigma_\theta = \frac{pD}{2t} \quad (7)$$

where p is the internal pressure, D is the pipe diameter and t is the wall thickness of the pipe [Reference 6]. The most accurate estimate of the average circumferential stress is found by using the inner diameter of the pipe in equation (7), but using the outer diameter in equation (7) provides a more conservative estimate. The circumferential stresses calculated using equation (7) are also shown in figures 34 and 37.

D. REFERENCES

1. Materials Laboratory Factual Report 10-119, National Transportation Safety Board, Washington, DC, 2011.
2. Materials Laboratory Factual Report 11-059, National Transportation Safety Board, Washington, DC, 2011.
3. Materials Laboratory Factual Report 11-056, National Transportation Safety Board, Washington, DC, 2011.
4. M.F. Ashby and D.R.H. Jones, Engineering Materials 1, An Introduction to their Properties and Applications, Pergamon Press, Oxford, 1980.
5. S.P. Timoshenko and J.N. Goodier, Theory of Elasticity, Third Edition, McGraw-Hill Book Company, New York, 1970.
6. R.J. Roark and W.C. Young, Formulas for Stress and Strain, Fifth Edition, McGraw-Hill Book Company, New York, 1975.

Carl R. Schultheisz
Materials Research Engineer

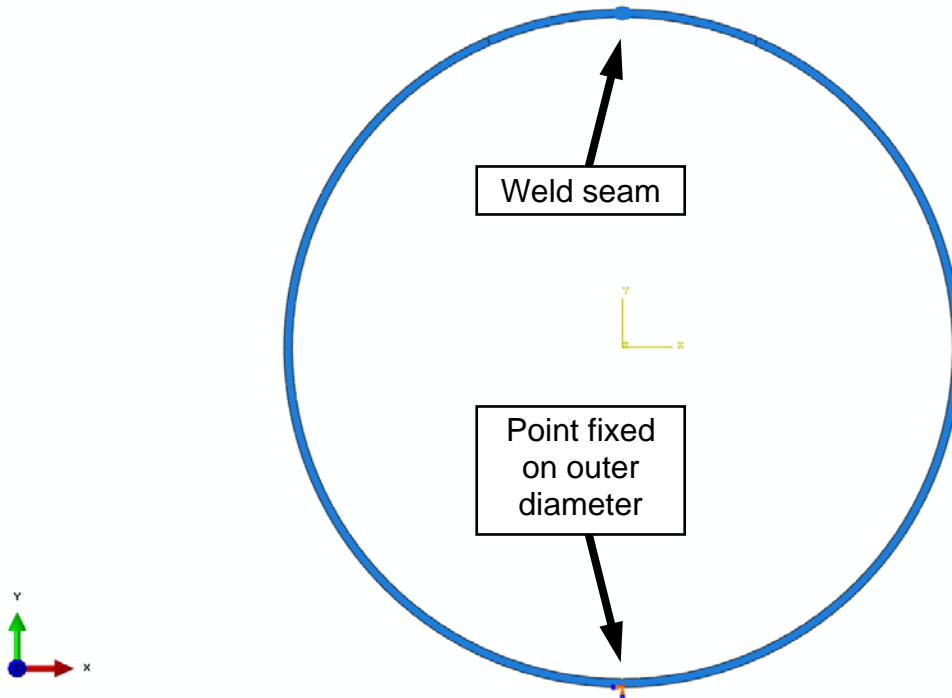


Figure 1. Overview of Model 1, the pipe with a DSAW seam having no defects.

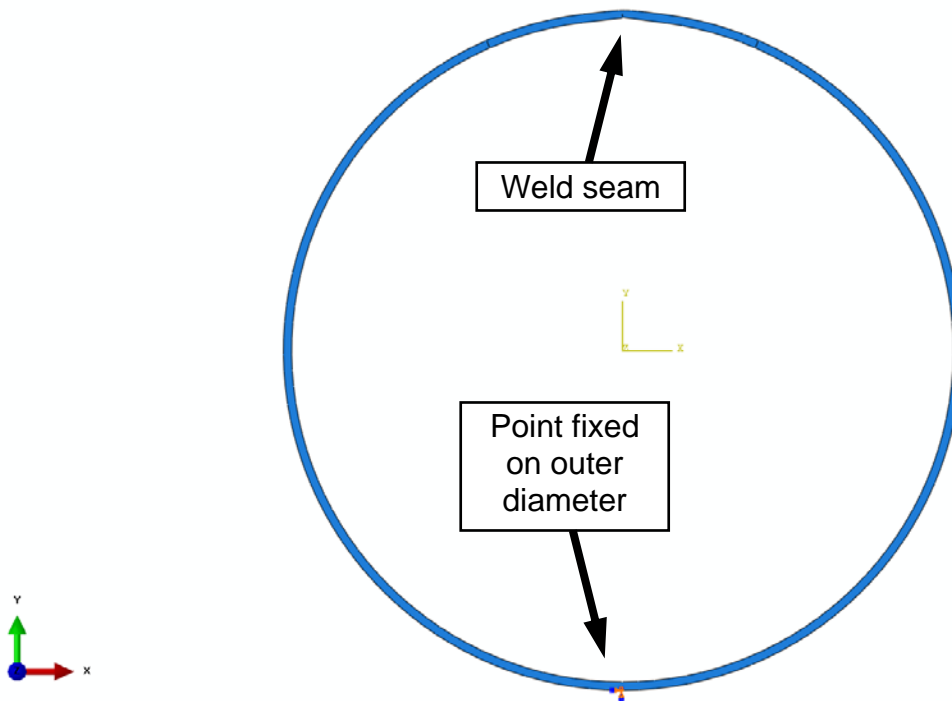


Figure 2. Overview of Model 2, the pipe having a welded seam with incomplete penetration.

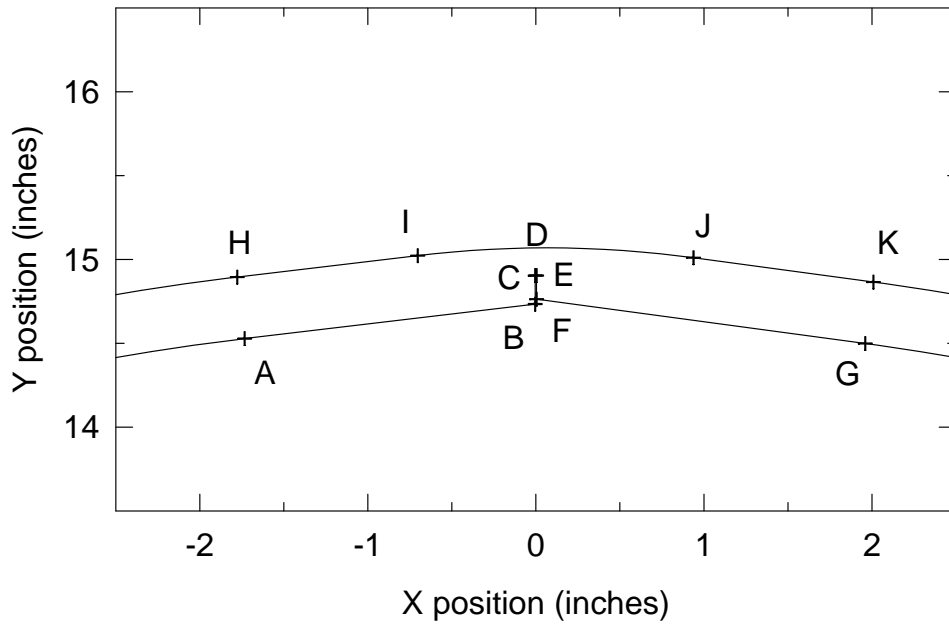


Figure 3. Sketch of the geometry of the weld seam with incomplete penetration for Model 2. The coordinates of the labeled control points are given in table 1.

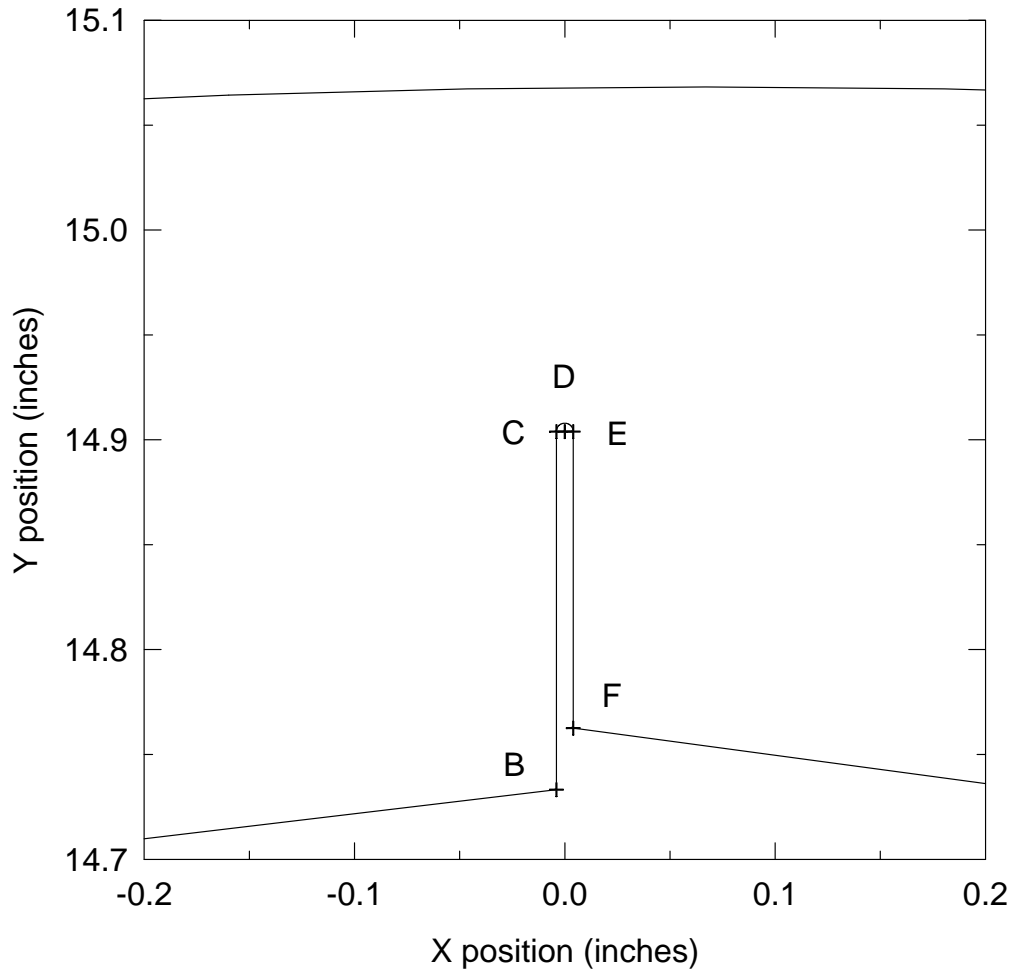


Figure 4. Closer view of the notch formed by the incomplete penetration of the weld in Model 2. The coordinates of the labeled control points are given in table 1.

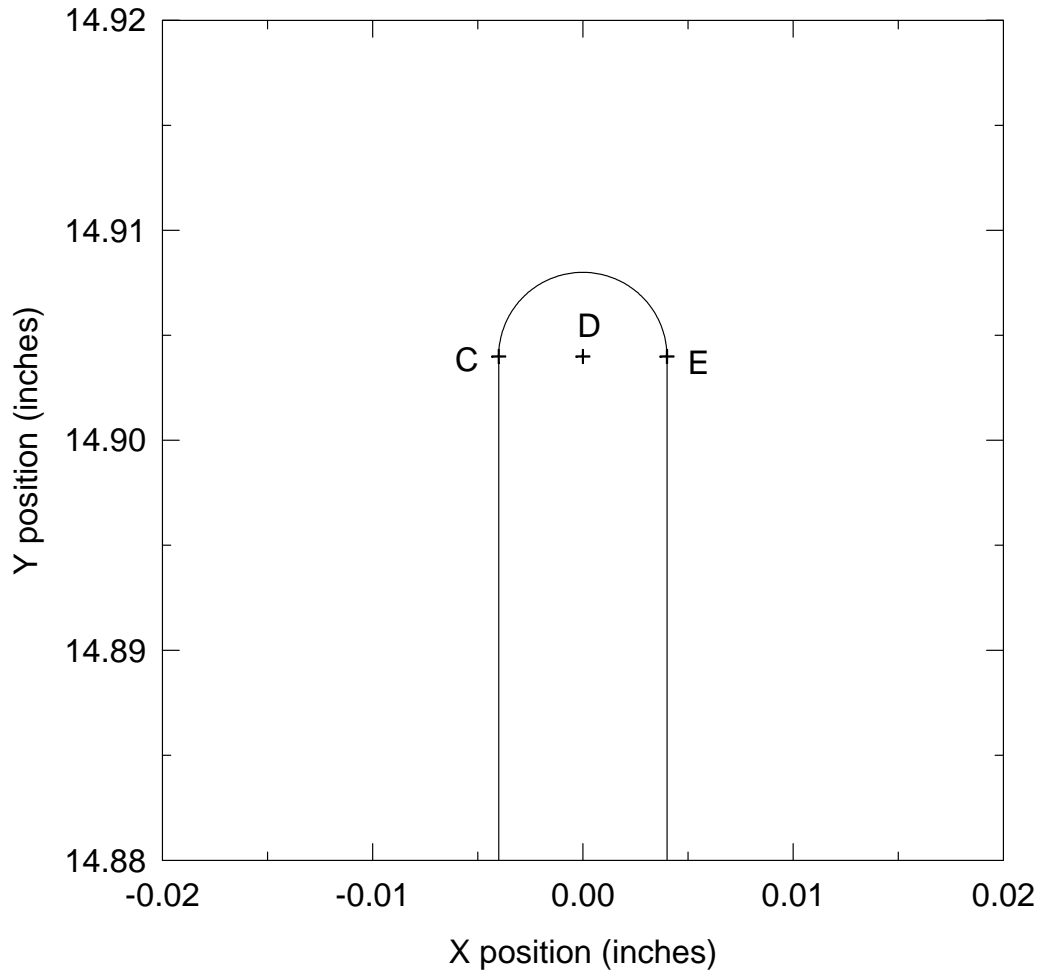


Figure 5. Closer view of the notch formed by the incomplete penetration of the weld in Model 2, showing the semicircular notch tip geometry. The coordinates of the labeled control points are given in table 1.

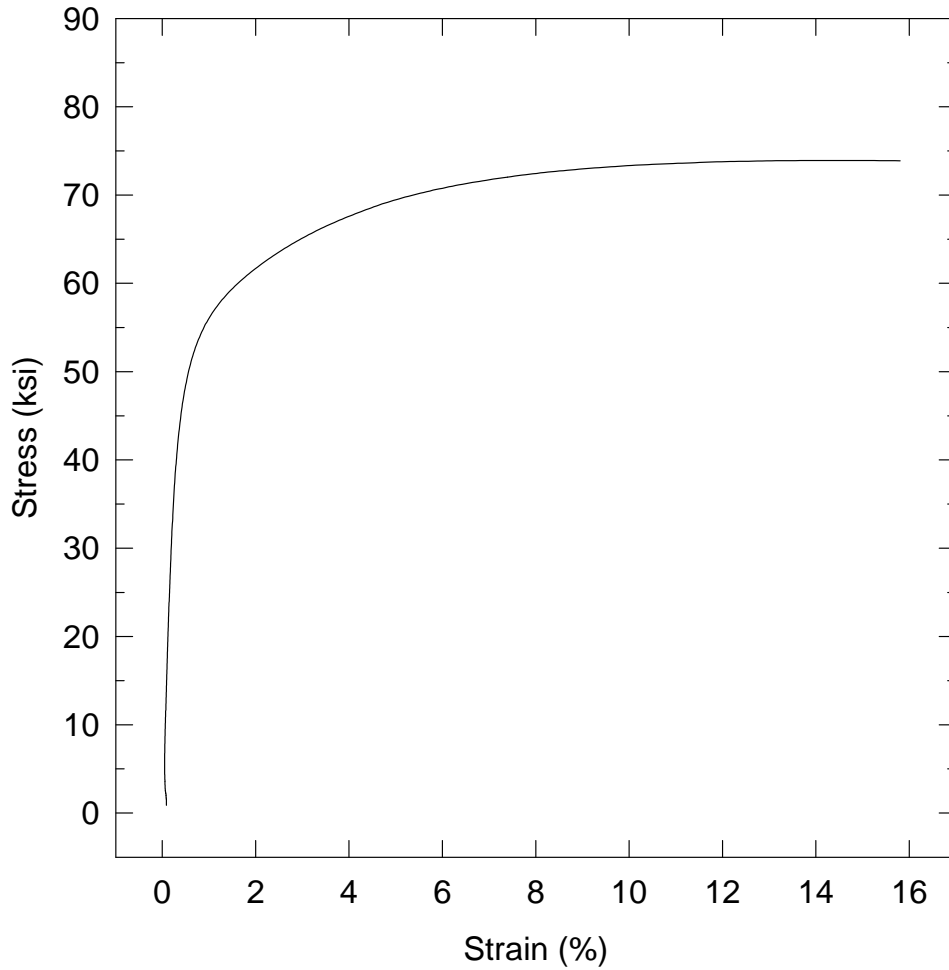


Figure 6. Measured uniaxial engineering stress versus strain data from a section of pipe some 700 feet upstream of the rupture, which was used as a basis for the stress-strain data input to the finite element models.

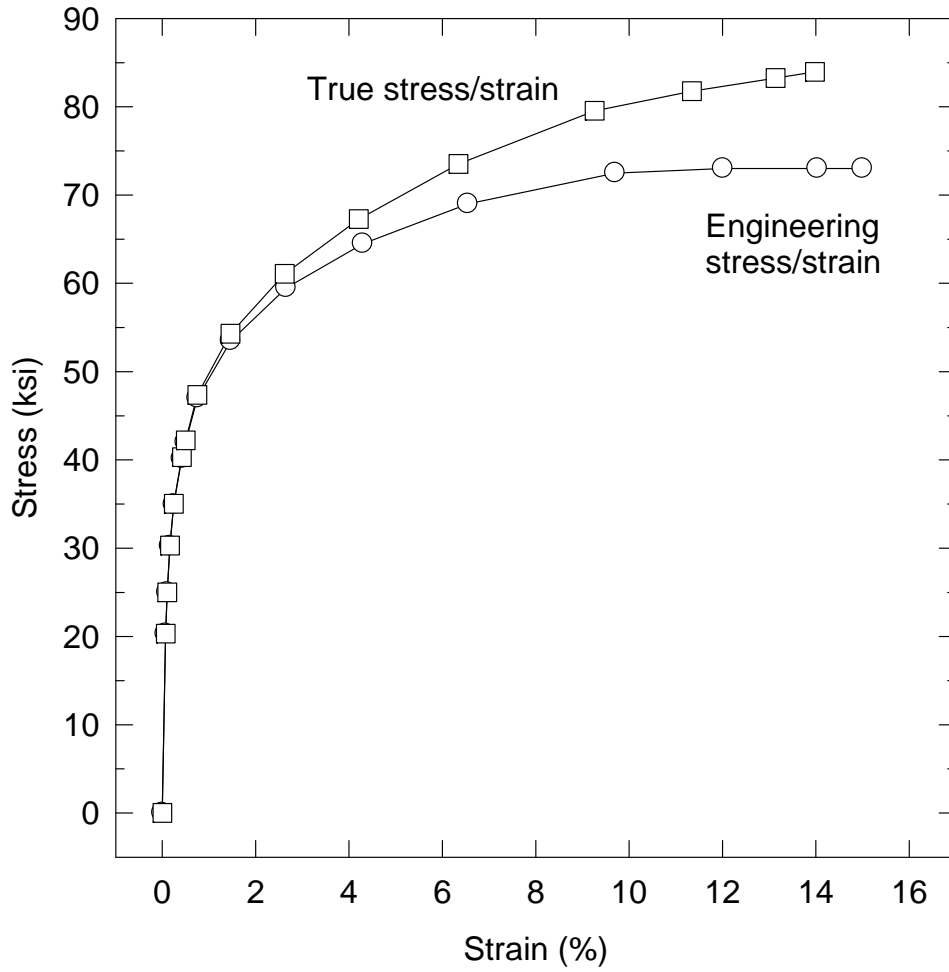


Figure 7. The true stress/strain data input to the finite element models, which is listed in table 2, along with the corresponding engineering stress/strain data based on the data in figure 6.

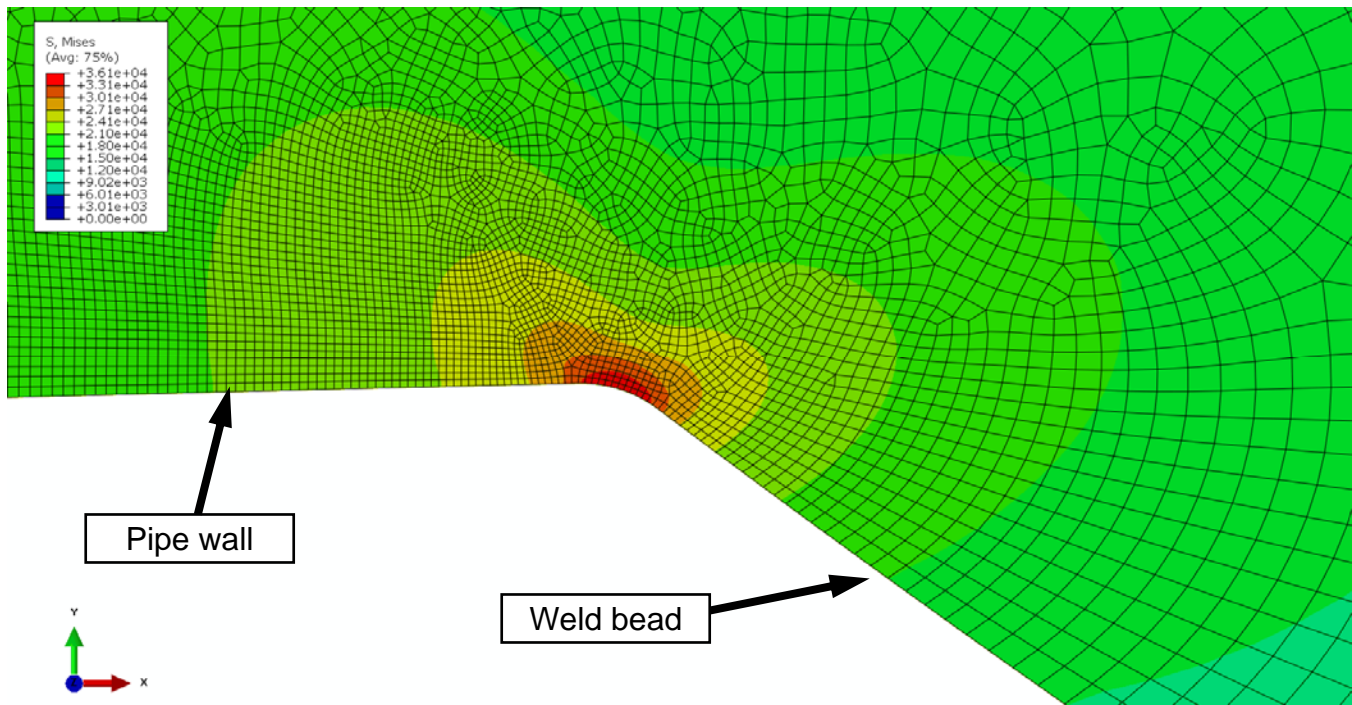


Figure 8. Mesh detail at one interior corner of the weld bead for Model 1, which has a weld seam with no defect. The radius of curvature at the corner is 0.004 inch, and the smallest element dimension is approximately 0.0002 inch.

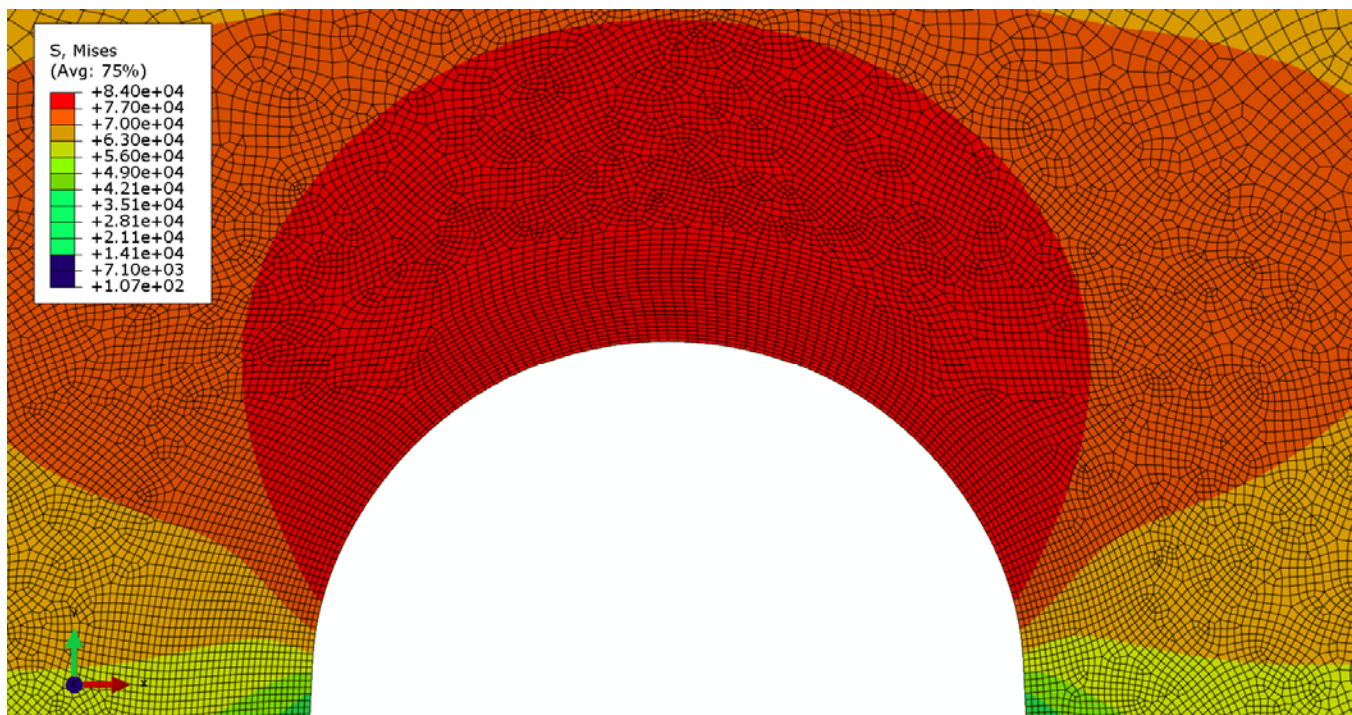


Figure 9. Mesh detail at the notch tip of Model 2, which has a weld seam with incomplete penetration. The notch tip radius is 0.004 inch, and the smallest element dimension is approximately 0.0001 inch.

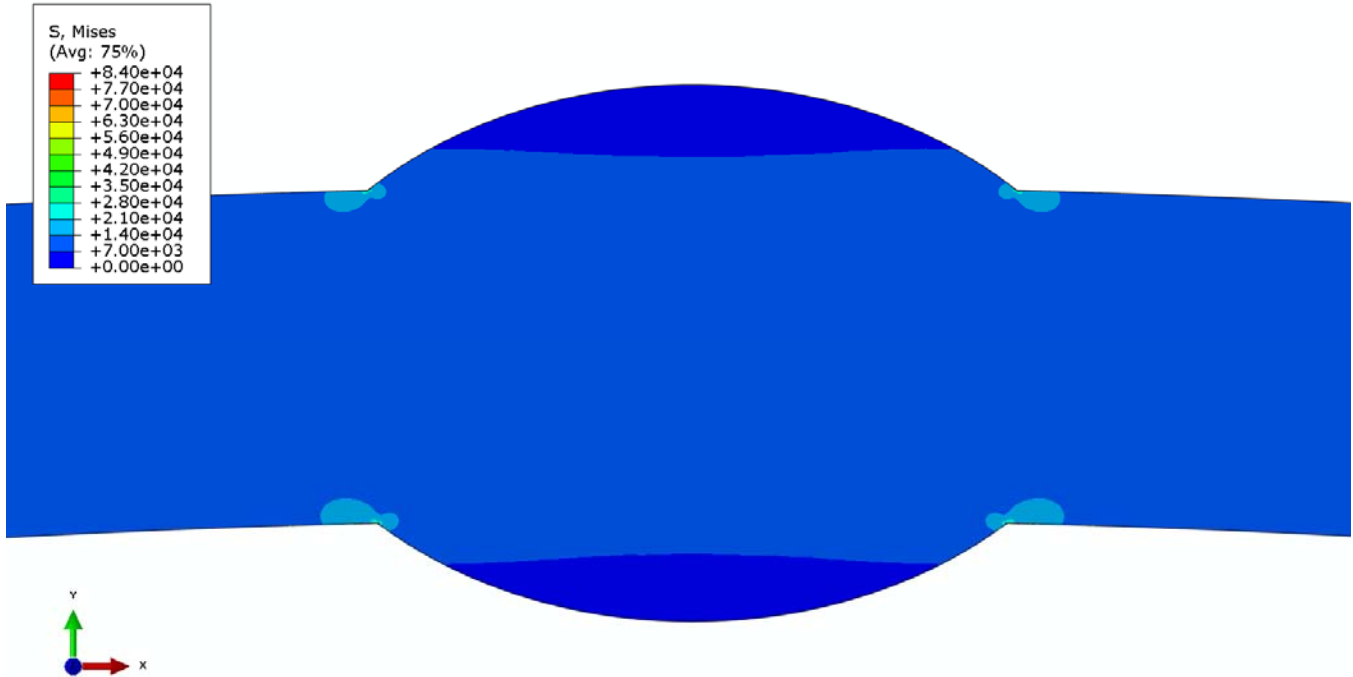


Figure 10. Contours of Mises stress at the seam weld with no defect in Model 1, at an internal pressure of 350 psi.



Figure 11. Contours of Mises stress at one interior corner of the weld bead in Model 1, at an internal pressure of 350 psi. Magnified 6 times with respect to figure 10.

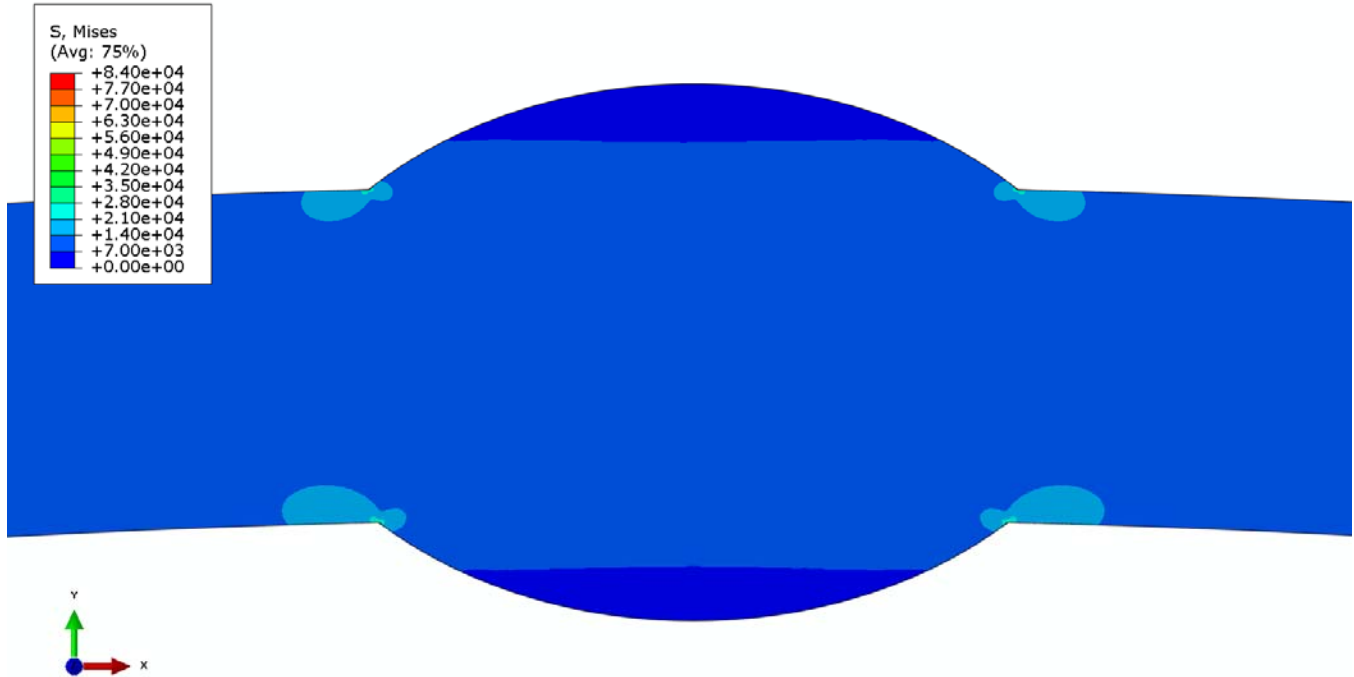


Figure 12. Contours of Mises stress at the seam weld with no defect in Model 1, at an internal pressure of 375 psi.



Figure 13. Contours of Mises stress at one interior corner of the weld bead in Model 1, at an internal pressure of 375 psi. Magnified 6 times with respect to figure 12.

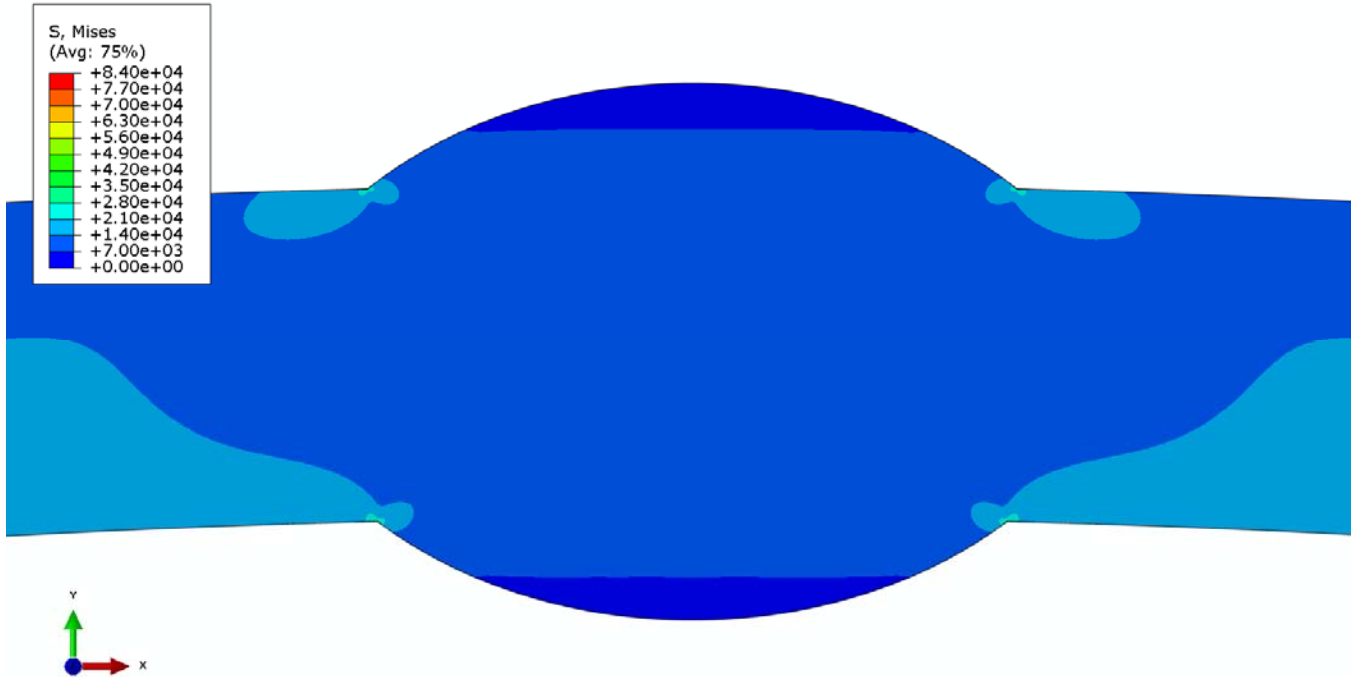


Figure 14. Contours of Mises stress at the seam weld with no defect in Model 1, at an internal pressure of 400 psi.

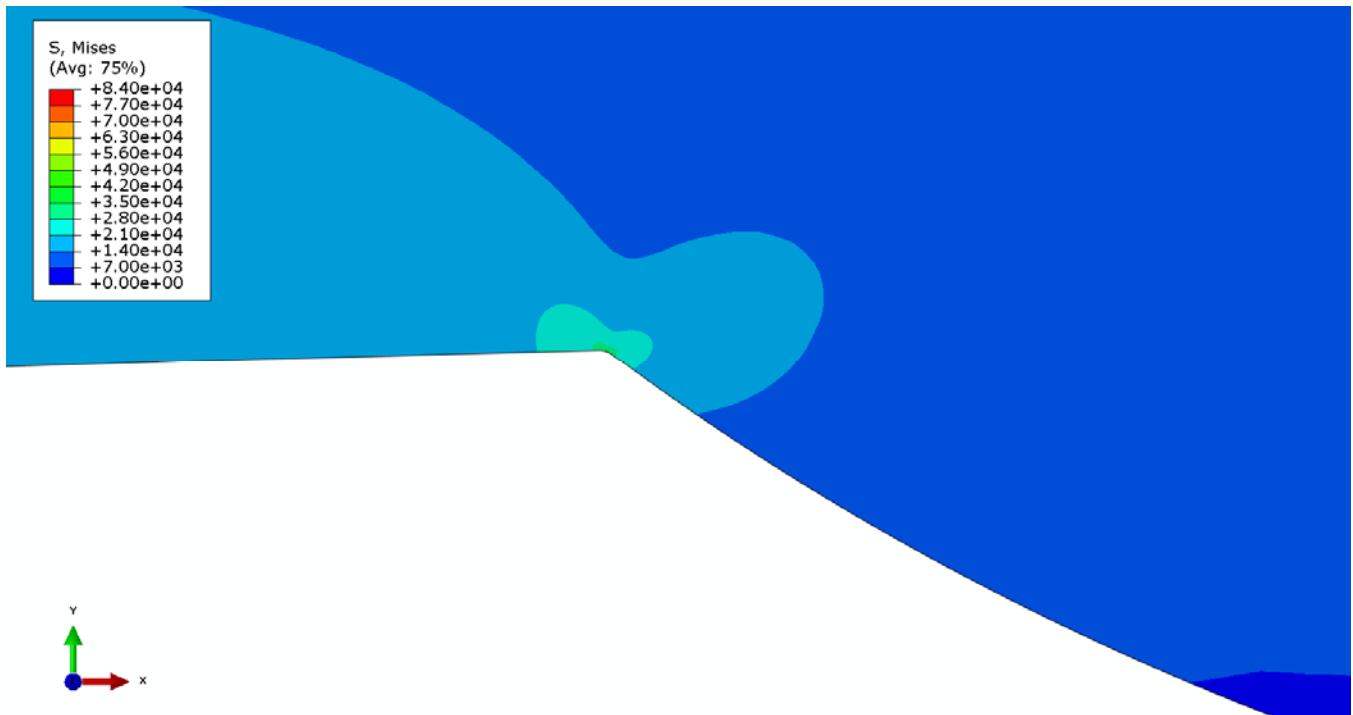


Figure 15. Contours of Mises stress at one interior corner of the weld bead in Model 1, at an internal pressure of 400 psi. Magnified 6 times with respect to figure 14.

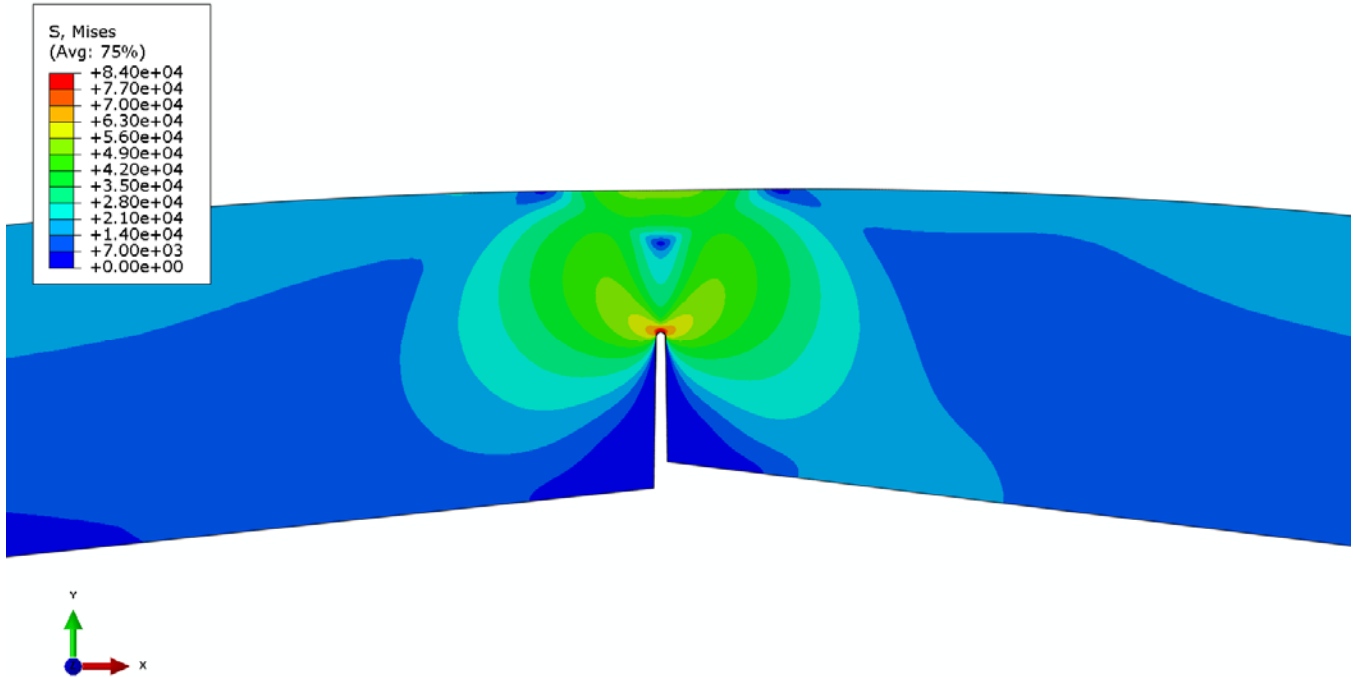


Figure 16. Contours of Mises stress at the seam weld with incomplete penetration in Model 2, at an internal pressure of 350 psi.

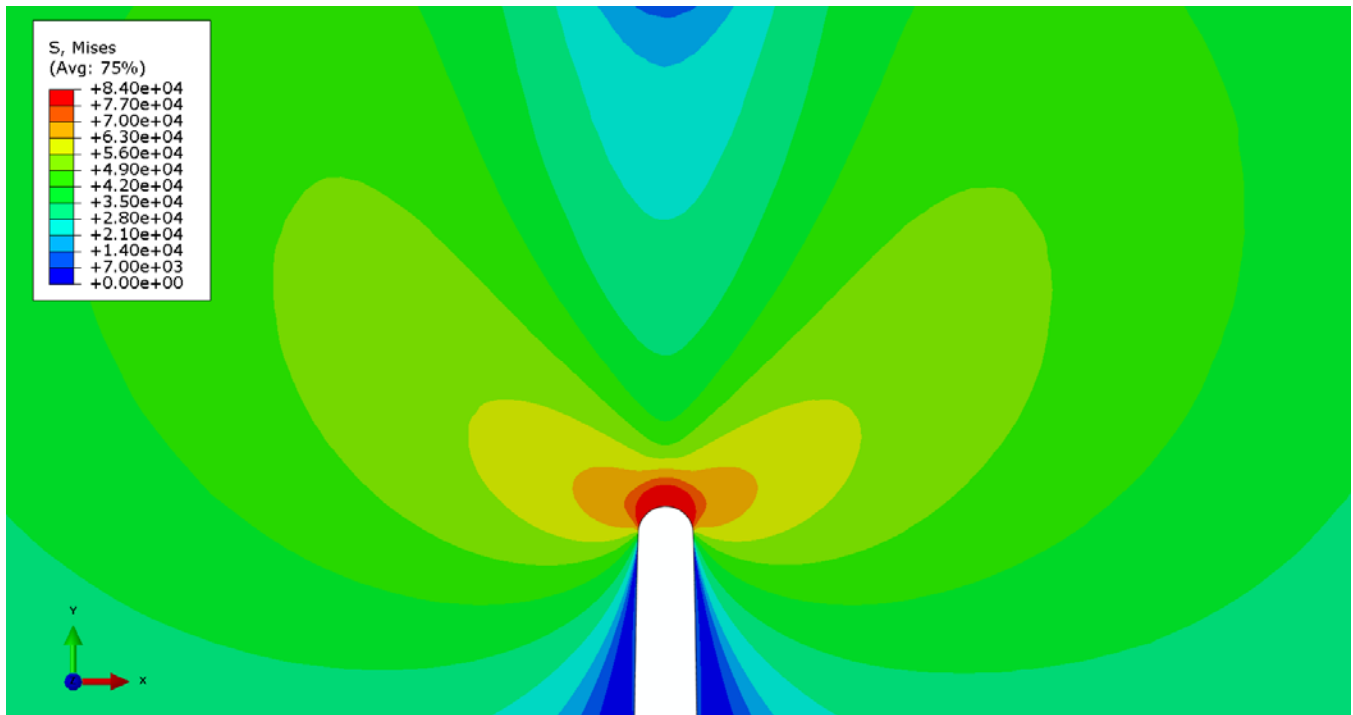


Figure 17. Contours of Mises stress at the notch formed by the incomplete penetration of the weld in Model 2, at an internal pressure of 350 psi. Magnified 6 times with respect to figure 16.

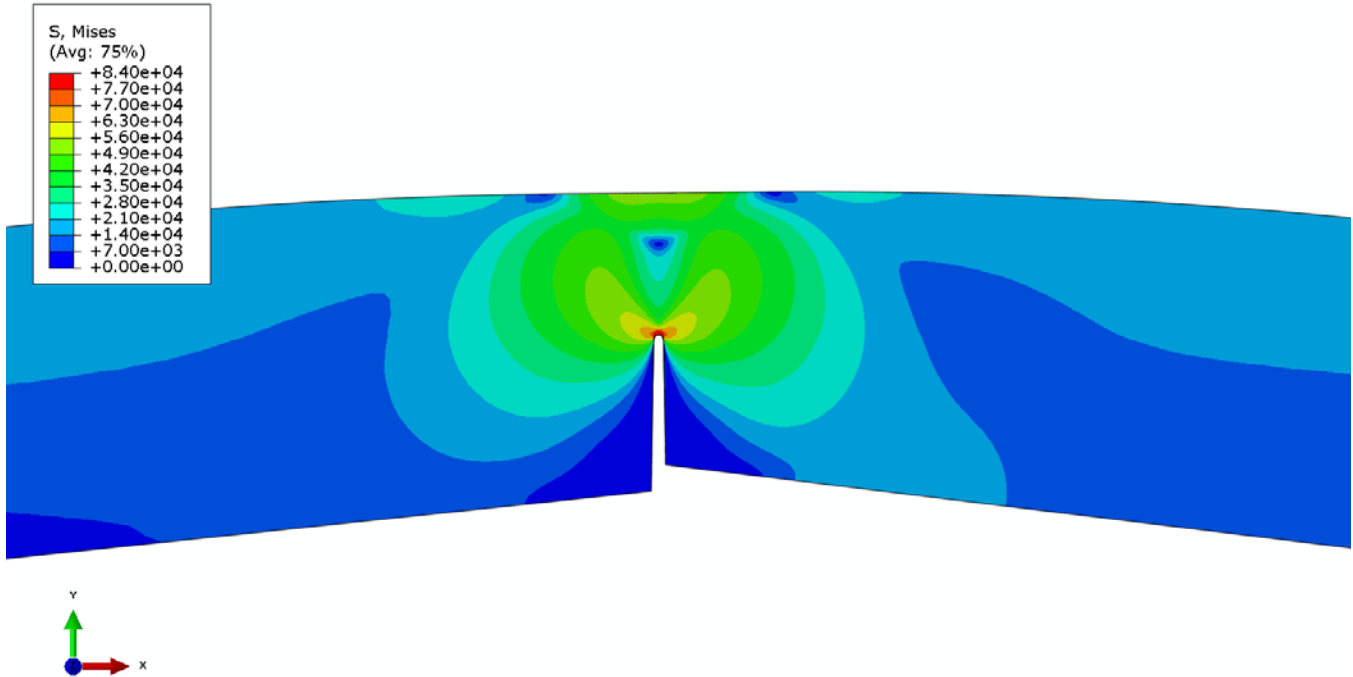


Figure 18. Contours of Mises stress at the seam weld with incomplete penetration in Model 2, at an internal pressure of 375 psi.

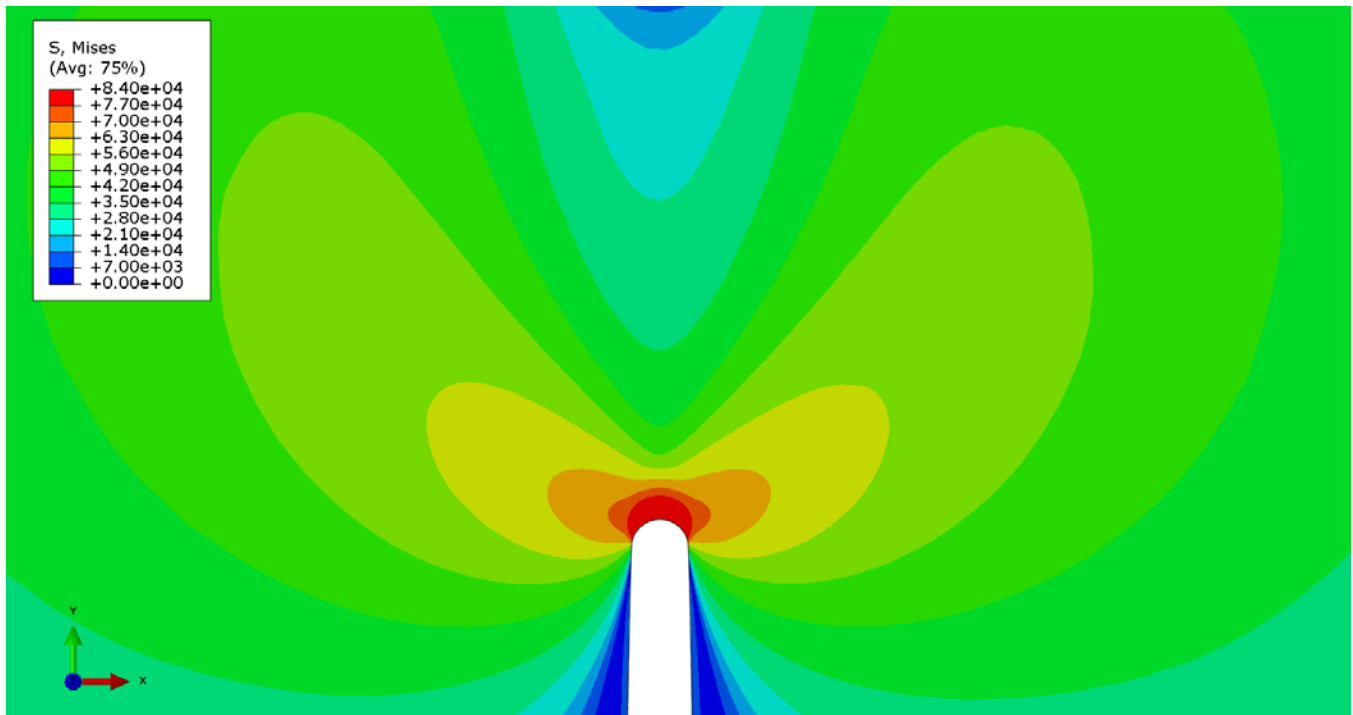


Figure 19. Contours of Mises stress at the notch formed by the incomplete penetration of the weld in Model 2, at an internal pressure of 375 psi. Magnified 6 times with respect to figure 18.

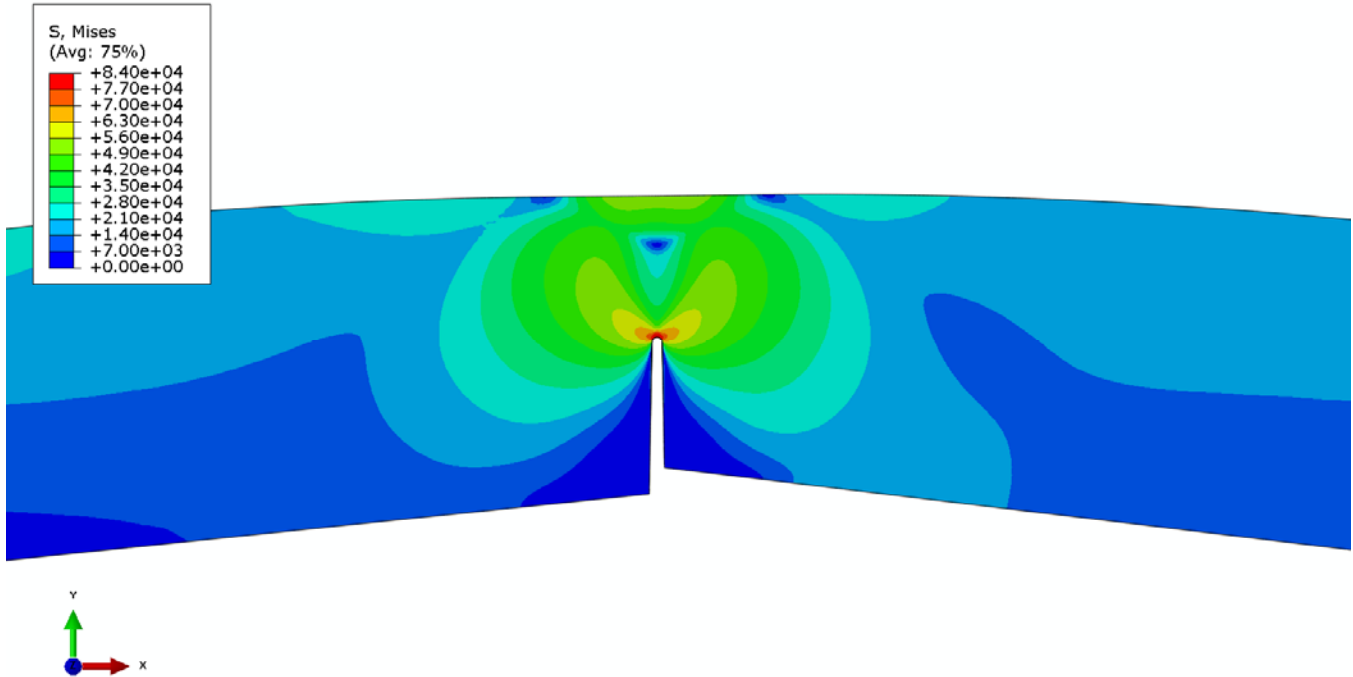


Figure 20. Contours of Mises stress at the seam weld with incomplete penetration in Model 2, at an internal pressure of 400 psi.

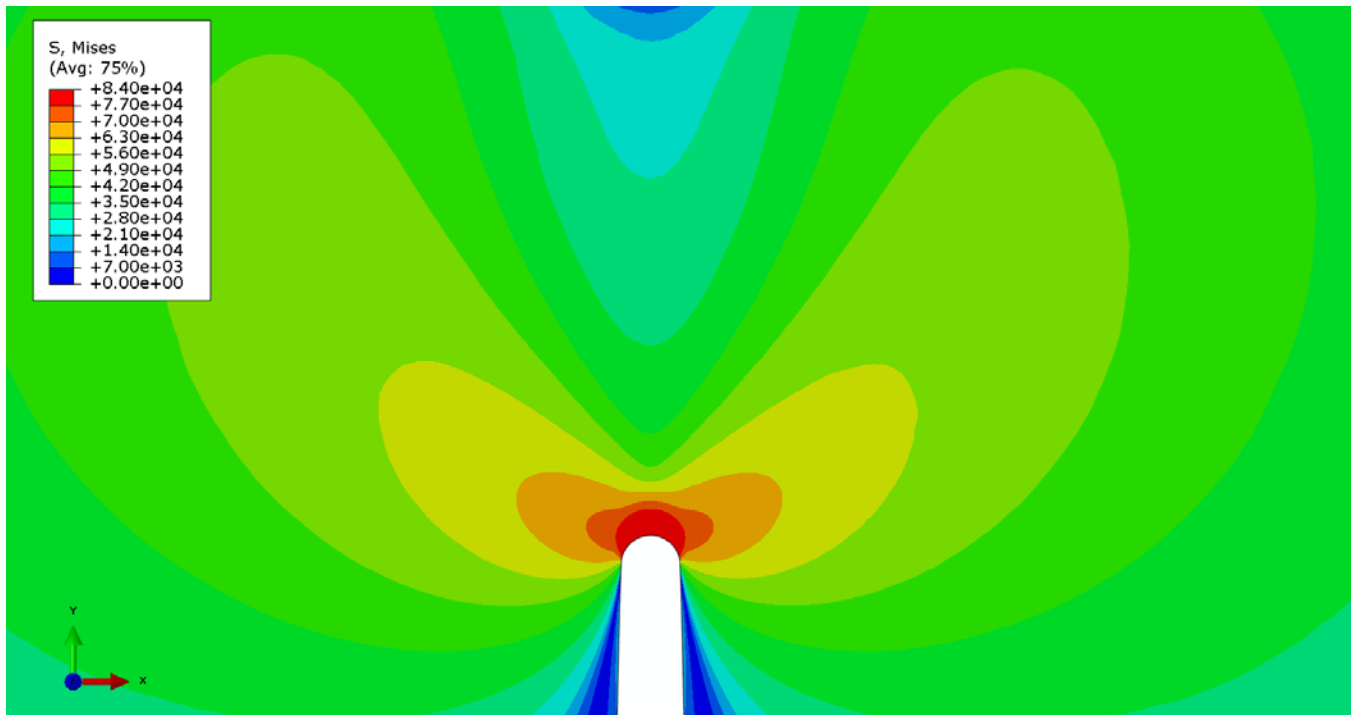


Figure 21. Contours of Mises stress at the notch formed by the incomplete penetration of the weld in Model 2, at an internal pressure of 400 psi. Magnified 6 times with respect to figure 20.

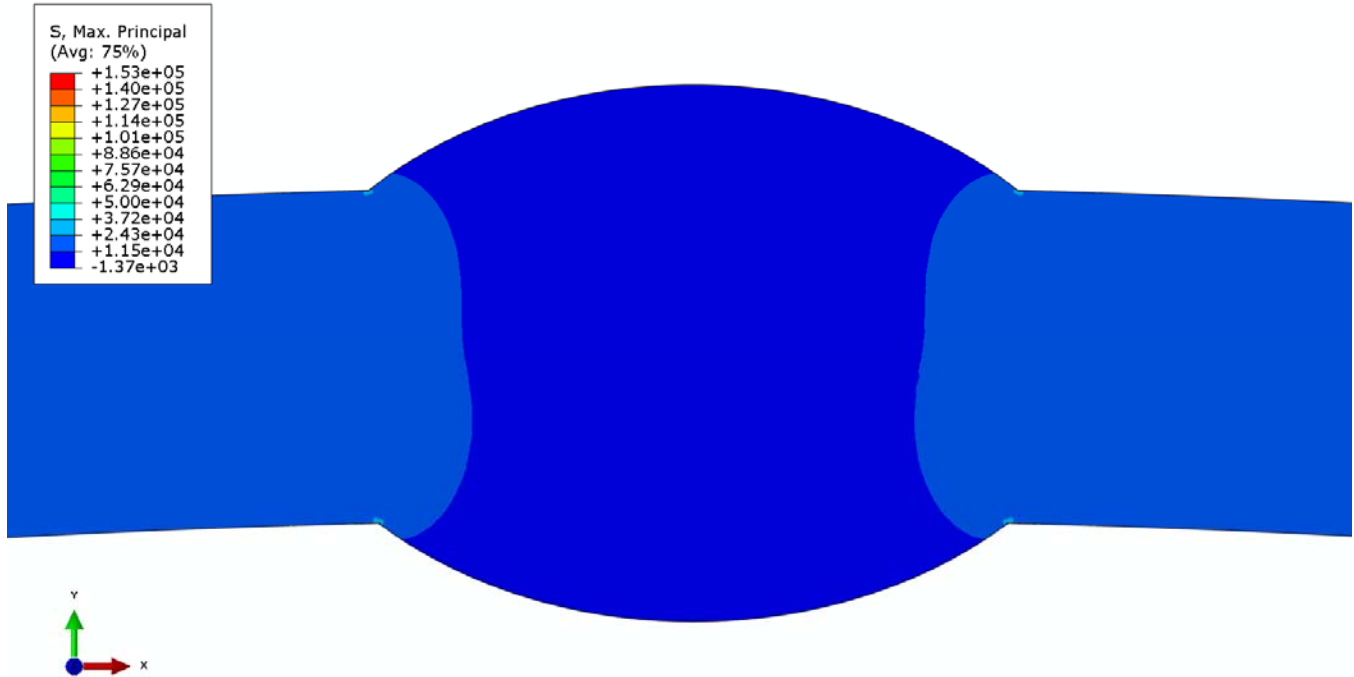


Figure 22. Contours of maximum principal stress at the seam weld with no defect in Model 1, at an internal pressure of 350 psi.

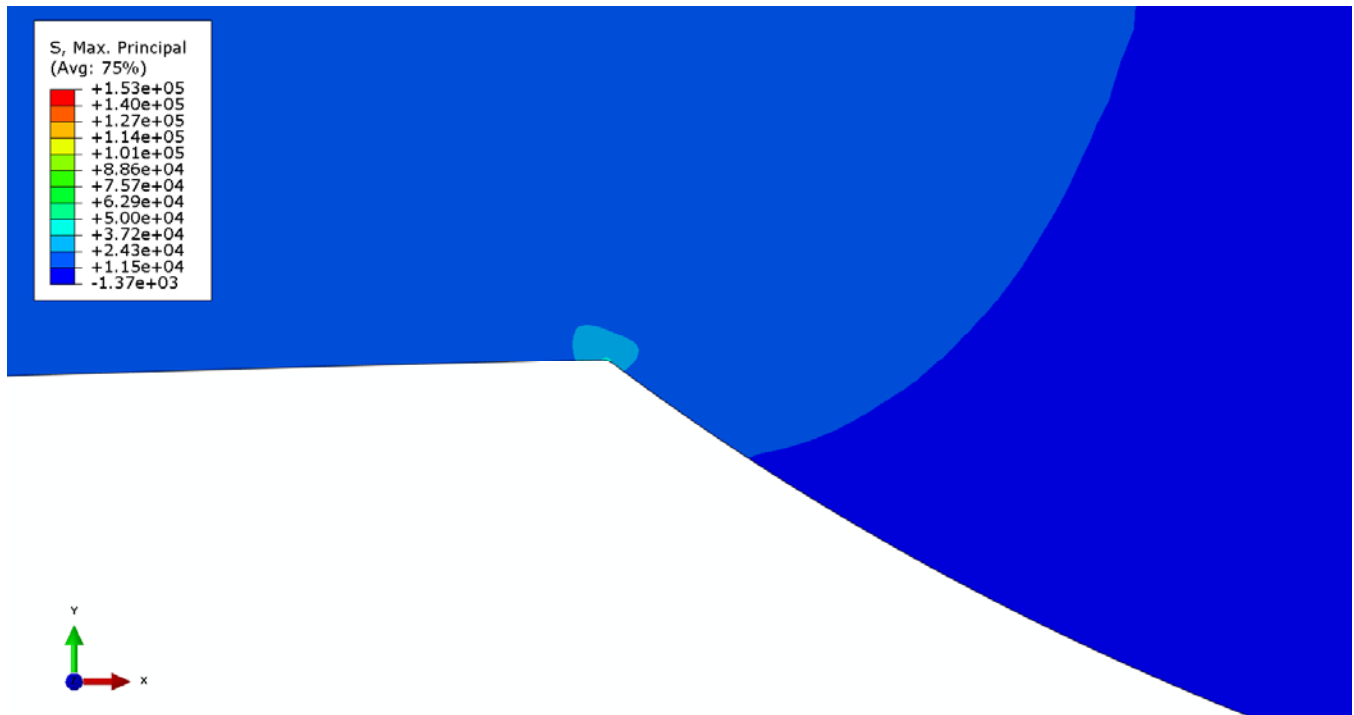


Figure 23. Contours of maximum principal stress at one interior corner of the weld bead in Model 1, at an internal pressure of 350 psi. Magnified 6 times with respect to figure 22.

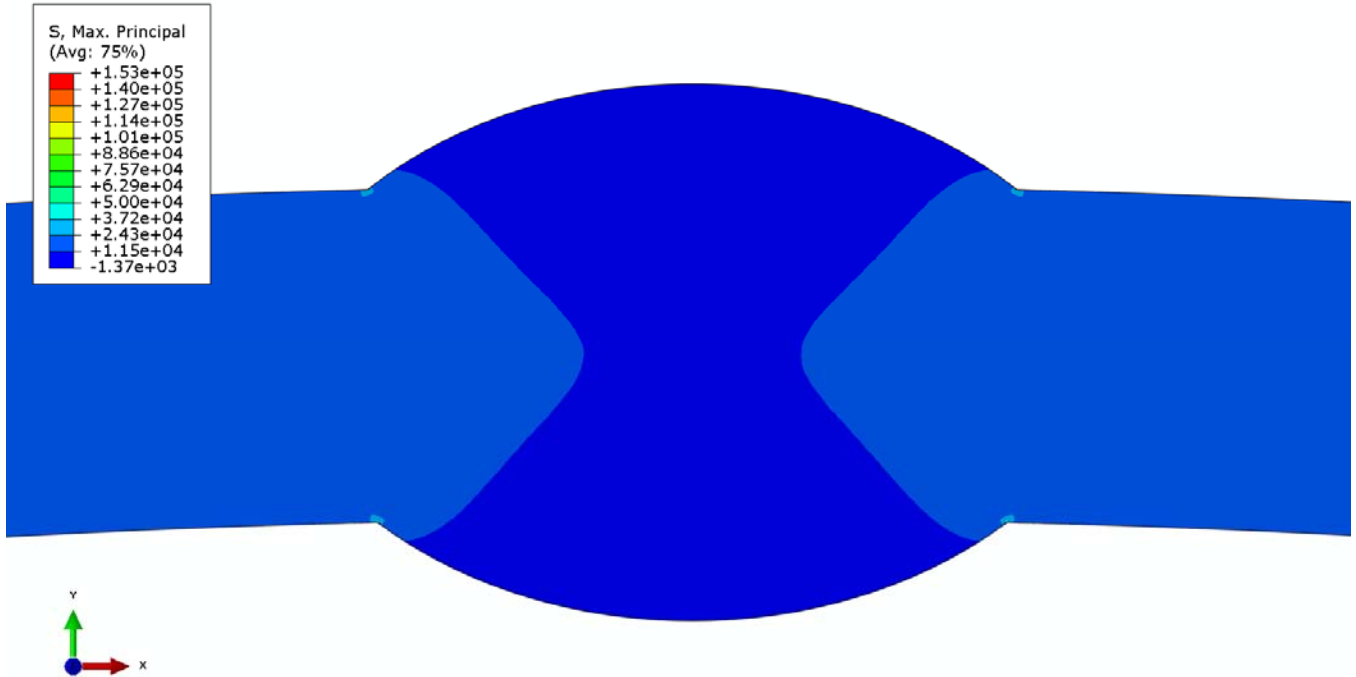


Figure 24. Contours of maximum principal stress at the seam weld with no defect in Model 1, at an internal pressure of 375 psi.

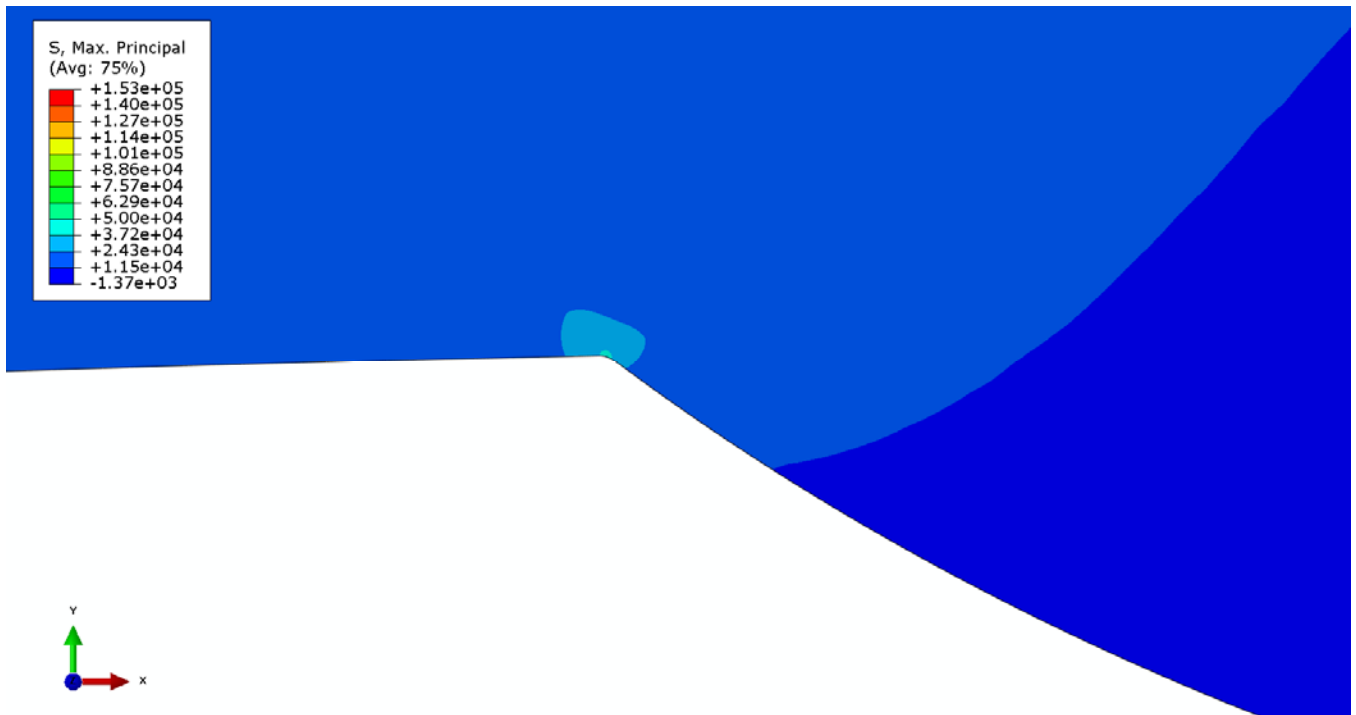


Figure 25. Contours of maximum principal stress at one interior corner of the weld bead in Model 1, at an internal pressure of 375 psi. Magnified 6 times with respect to figure 24.

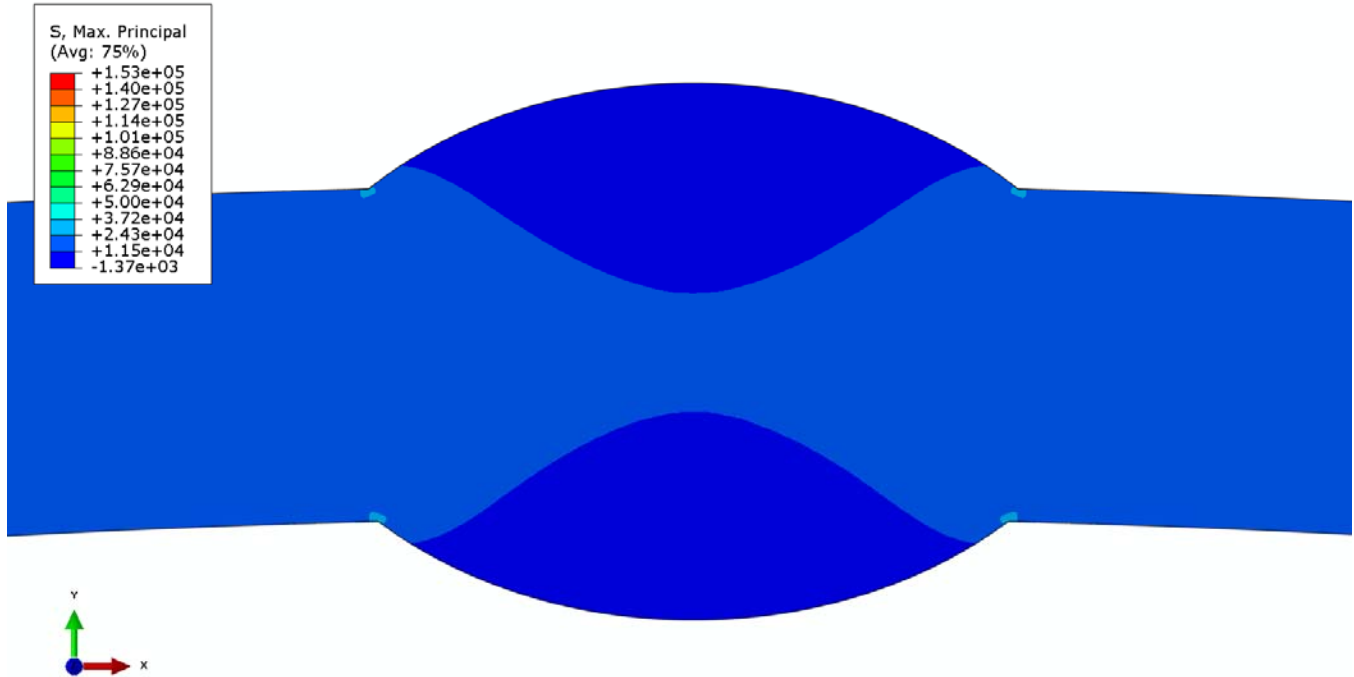


Figure 26. Contours of maximum principal stress at the seam weld with no defect in Model 1, at an internal pressure of 400 psi.

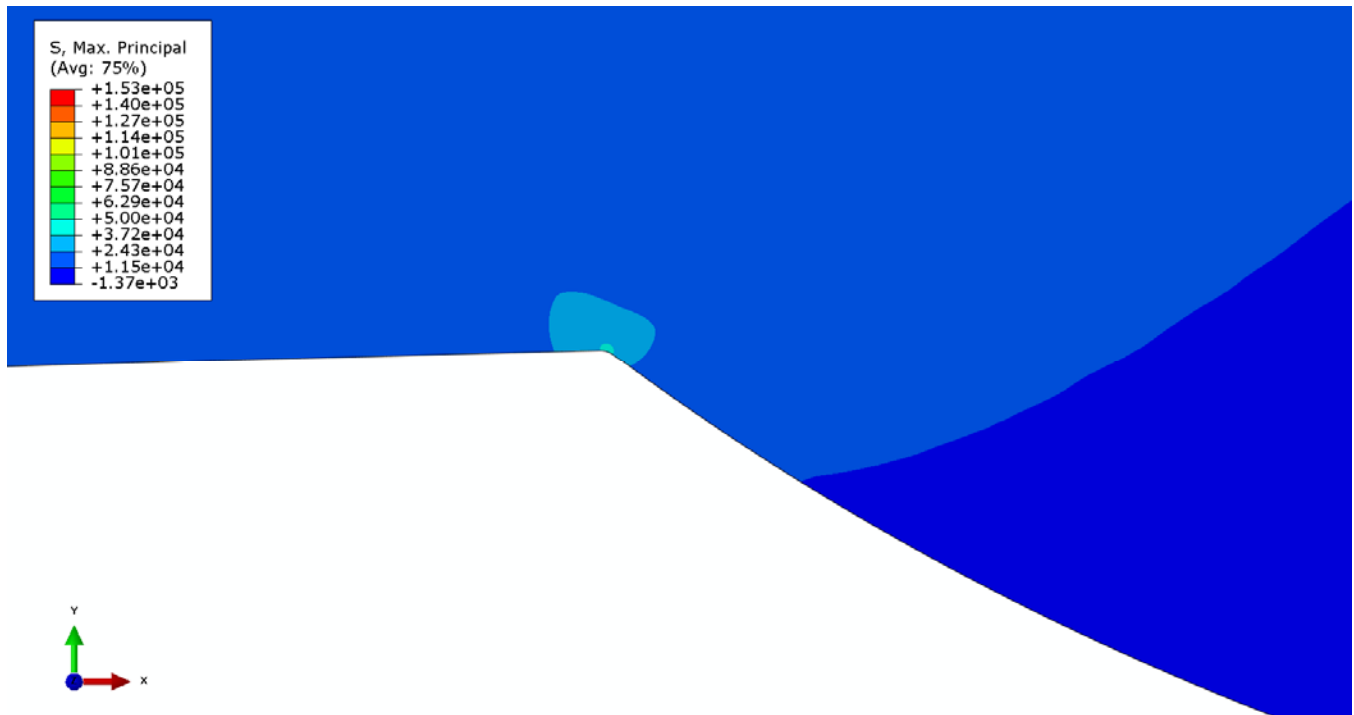


Figure 27. Contours of maximum principal stress at one interior corner of the weld bead in Model 1, at an internal pressure of 400 psi. Magnified 6 times with respect to figure 26.

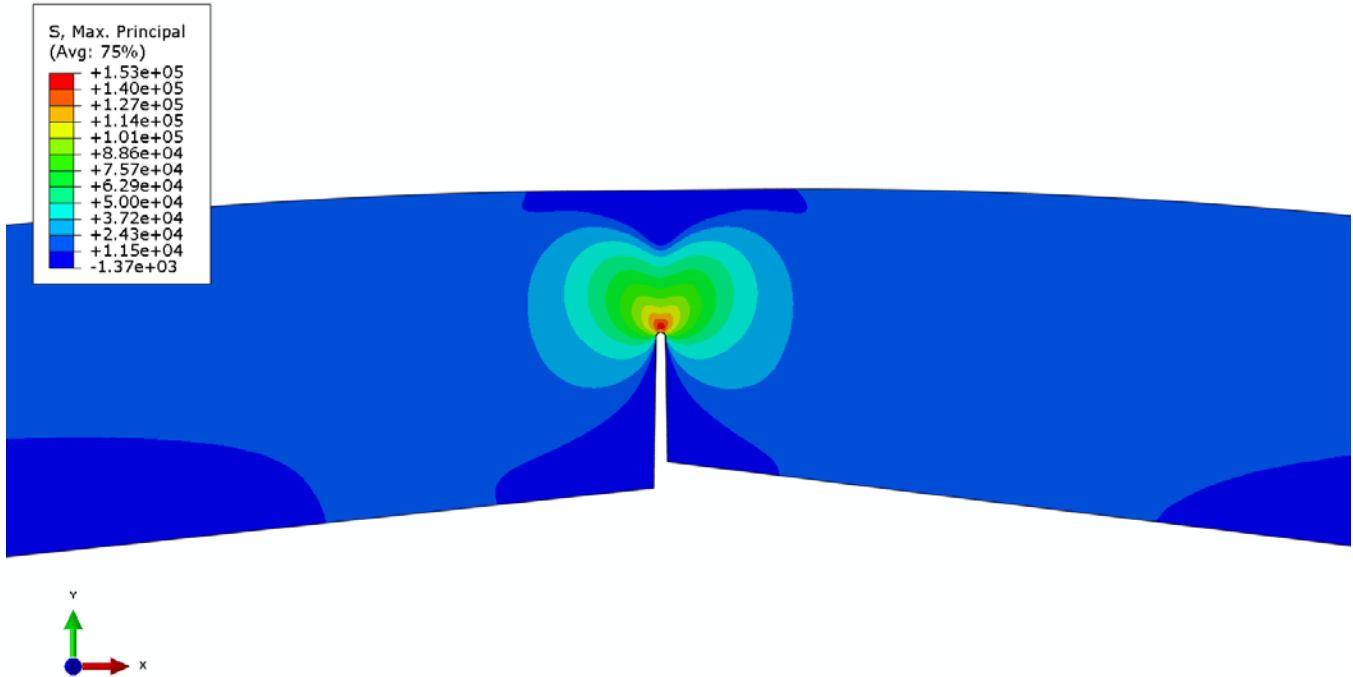


Figure 28. Contours of maximum principal stress at the seam weld with incomplete penetration in Model 2, at an internal pressure of 350 psi.

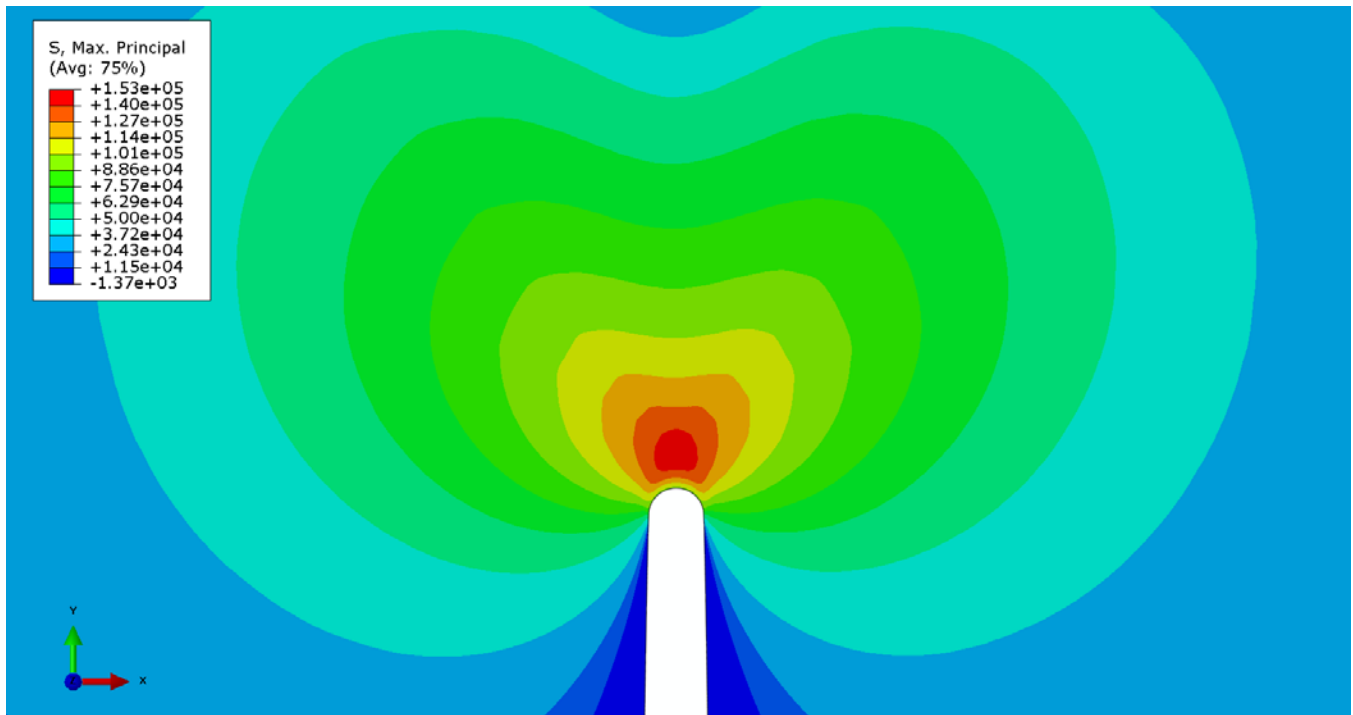


Figure 29. Contours of maximum principal stress at the notch formed by the incomplete penetration of the weld in Model 2, at an internal pressure of 350 psi. Magnified 6 times with respect to figure 28.

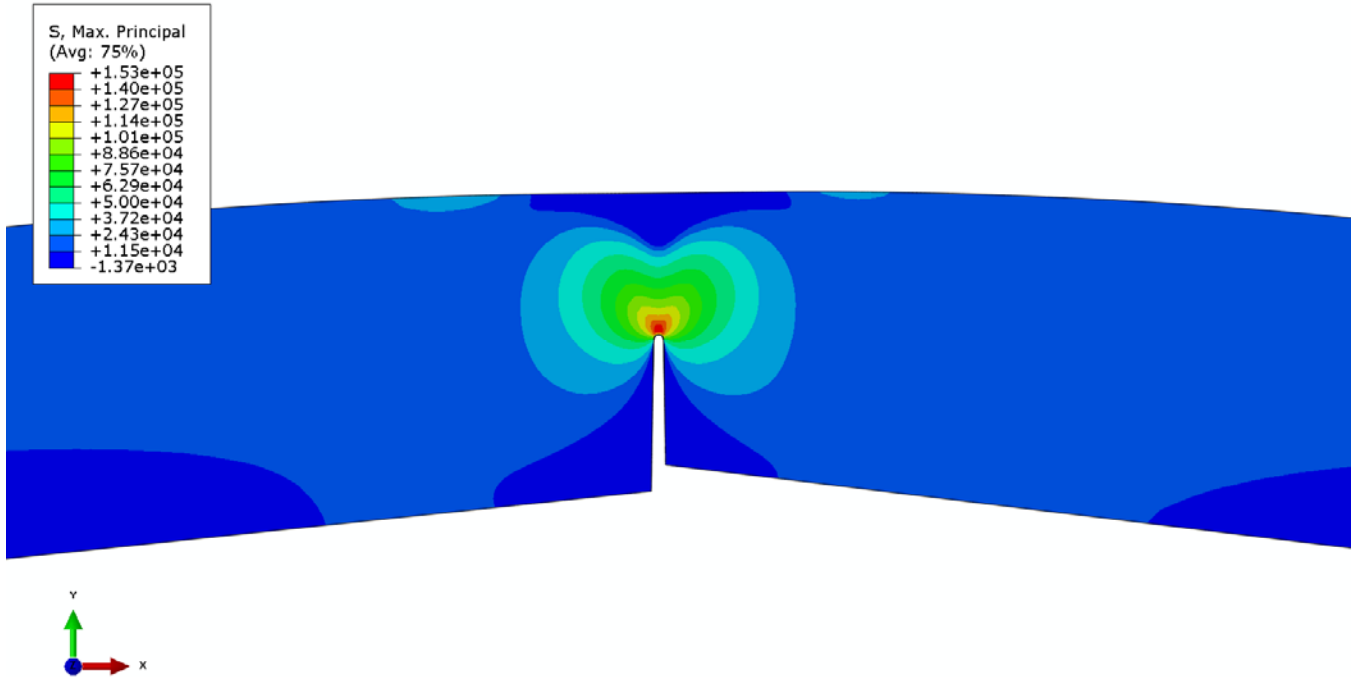


Figure 30. Contours of maximum principal stress at the seam weld with incomplete penetration in Model 2, at an internal pressure of 375 psi.

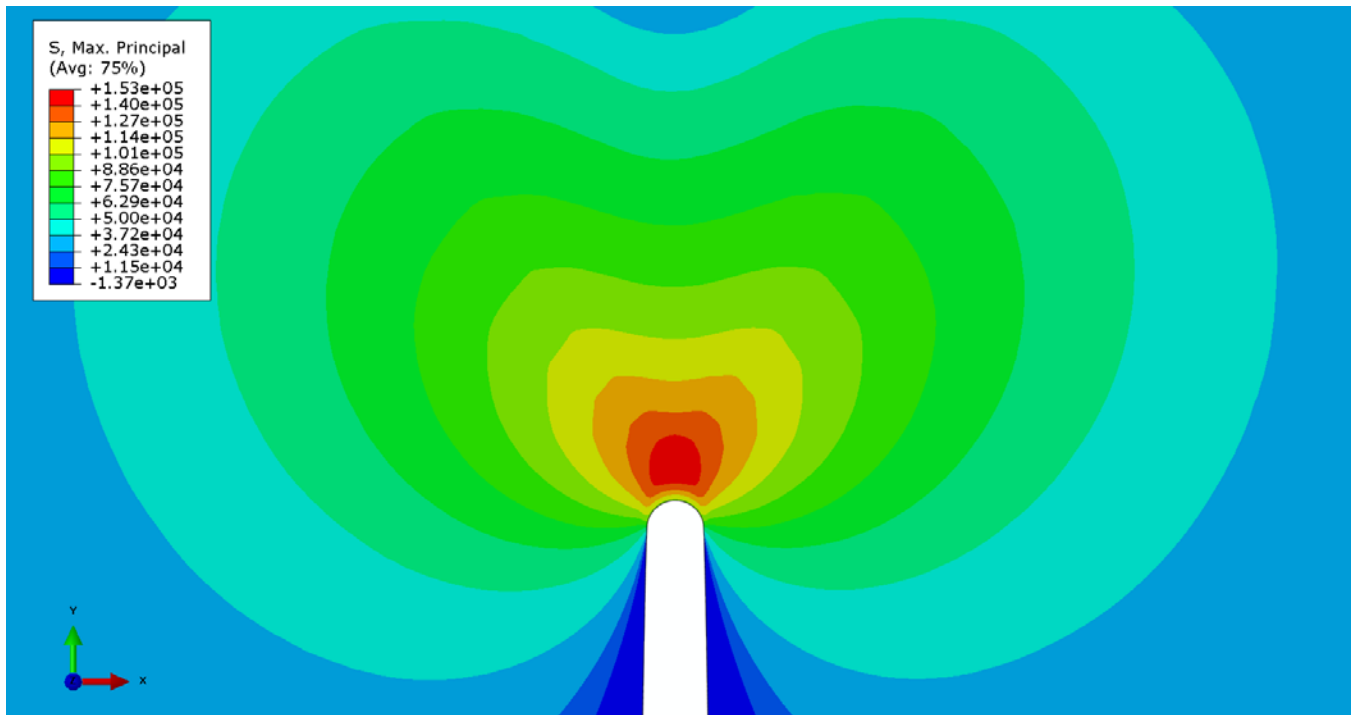


Figure 31. Contours of maximum principal stress at the notch formed by the incomplete penetration of the weld in Model 2, at an internal pressure of 375 psi. Magnified 6 times with respect to figure 30.

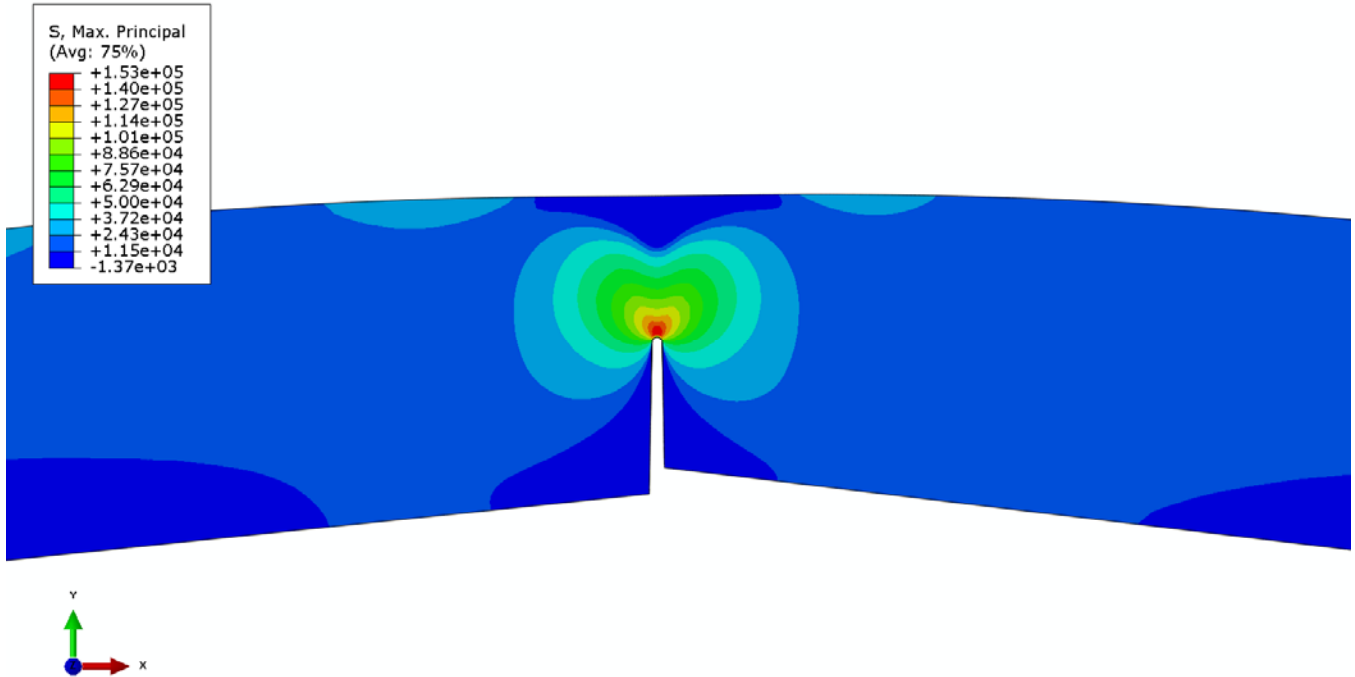


Figure 32. Contours of maximum principal stress at the seam weld with incomplete penetration in Model 2, at an internal pressure of 400 psi.

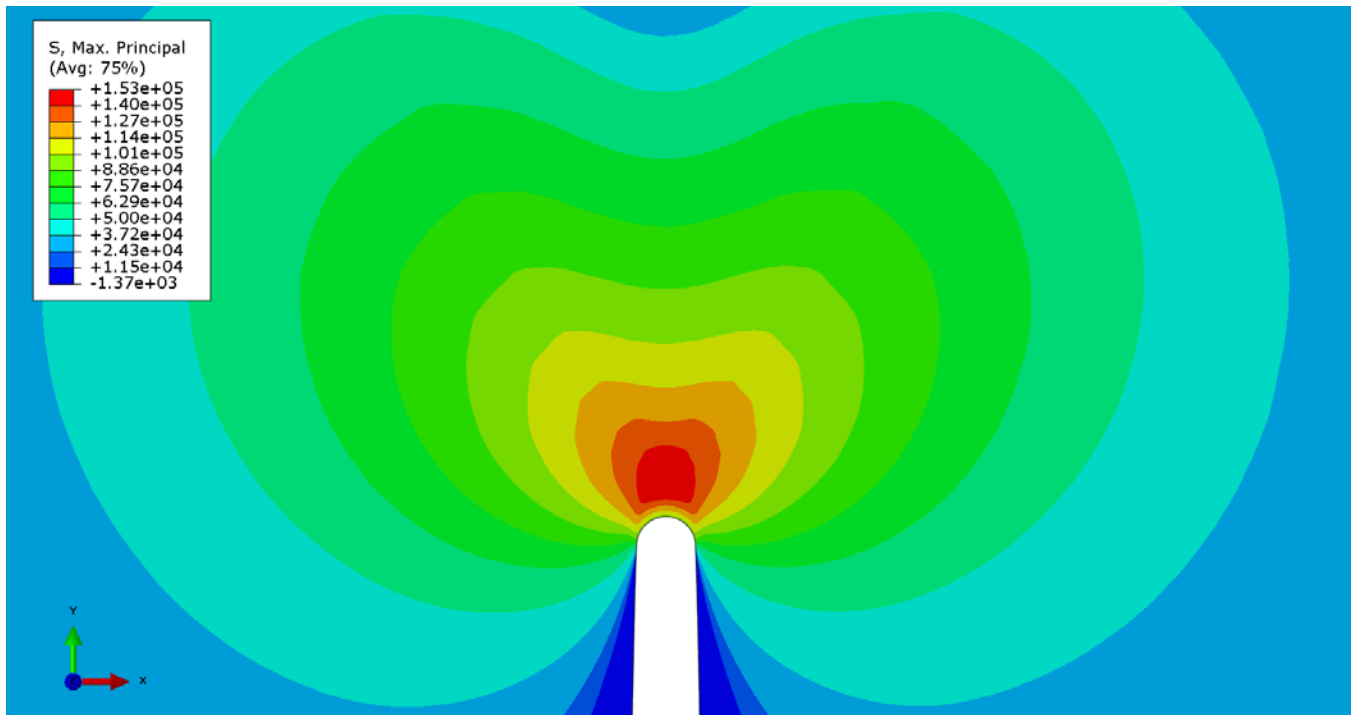


Figure 33. Contours of maximum principal stress at the notch formed by the incomplete penetration of the weld in Model 2, at an internal pressure of 400 psi. Magnified 6 times with respect to figure 32.

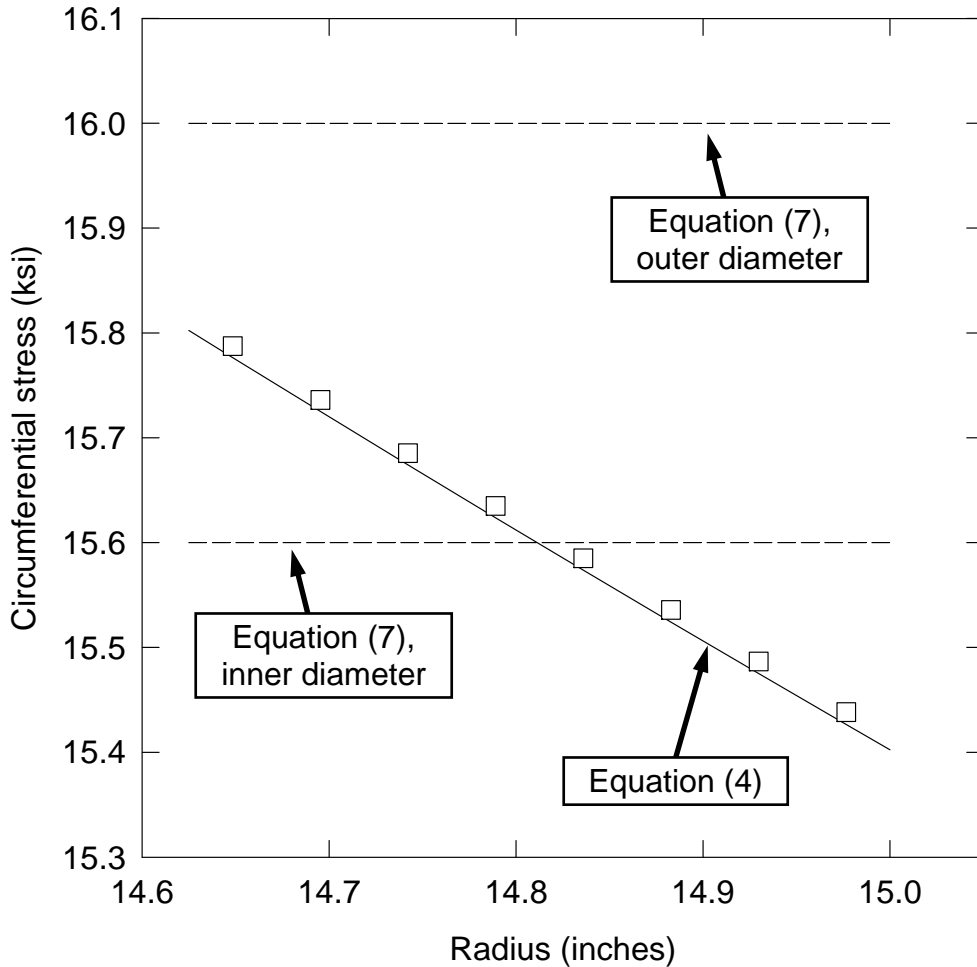


Figure 34. Circumferential stress in the pipe opposite the weld in Model 1, which has a welded seam with no defect. The internal pressure is 400 psi. Squares represent the stress at the central integration point along a radial row of elements. The solid line is equation (4), and the dashed lines are equation (7), referenced either to the inner or outer diameter of the pipe.

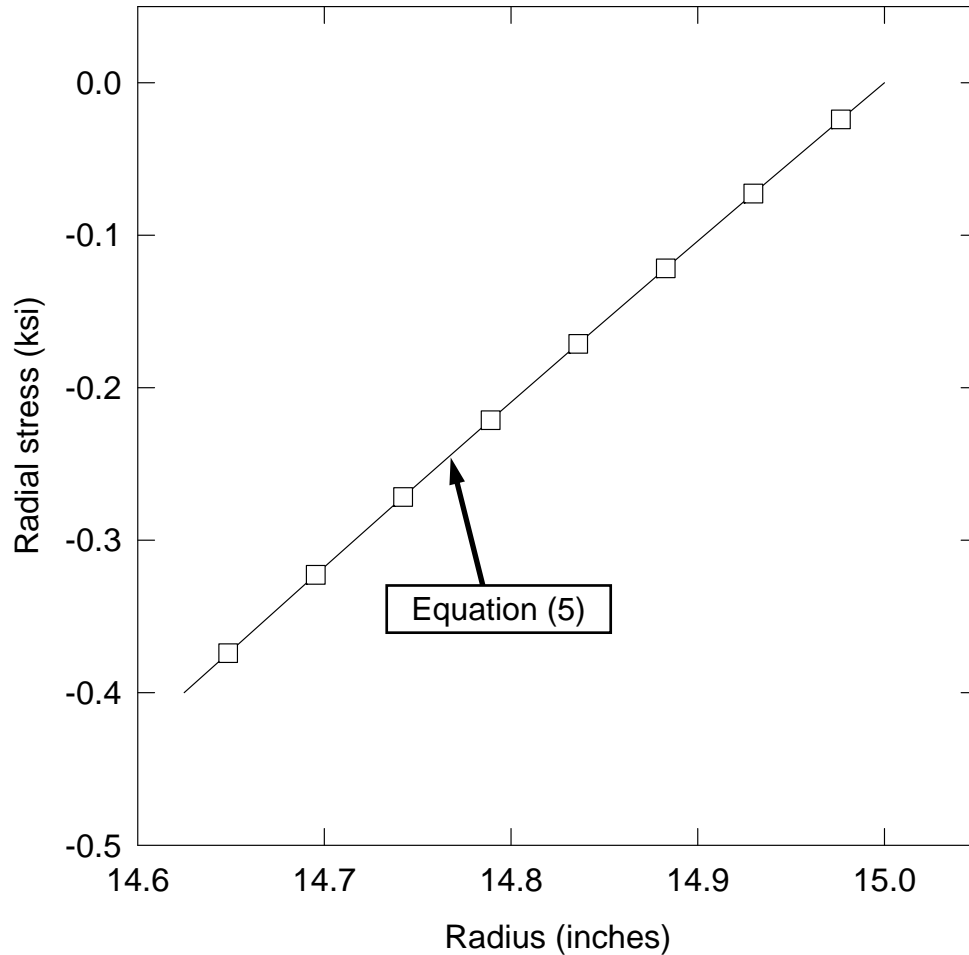


Figure 35. Radial stress in the pipe opposite the weld in Model 1, which has a welded seam with no defect. The internal pressure is 400 psi. Squares represent the stress at the central integration point along a radial row of elements. The solid line is equation (5). The radial stress is equal in magnitude to the pressure (400 psi or 0.4 ksi, with compressive stresses taken as negative) at the inner surface (a radius of 14.625 inches), and equal to zero at the outer surface (a radius of 15 inches).

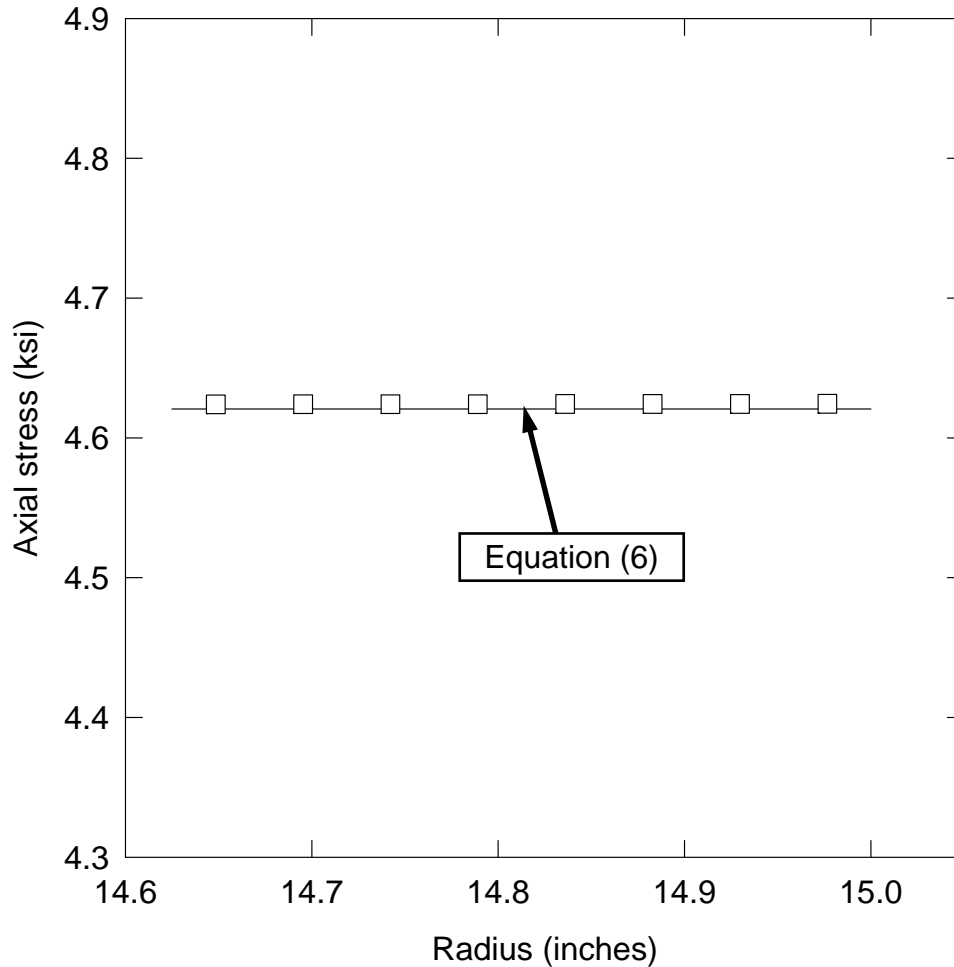


Figure 36. Axial stress in the pipe opposite the weld in Model 1, which has a welded seam with no defect. The internal pressure is 400 psi. Squares represent the stress at the central integration point along a radial row of elements. The solid line is equation (6). Because the radial stress is much smaller than the circumferential stress, the axial stress is approximately equal to Poisson's ratio times the average circumferential stress.

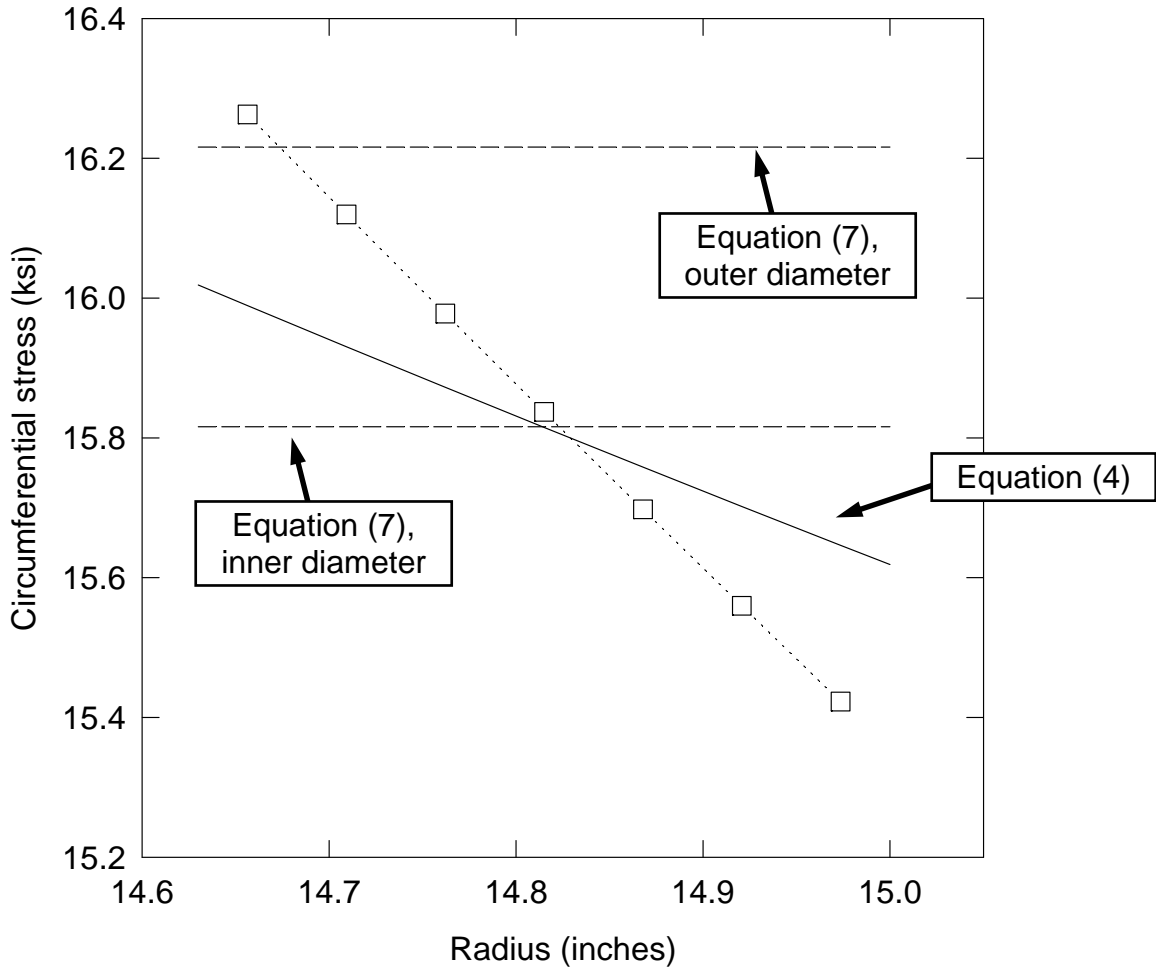


Figure 37 Circumferential stress in the pipe opposite the weld in Model 2, which has a welded seam with incomplete penetration. The internal pressure is 400 psi. Squares (connected by a dotted line to aid in tracking the data) represent the stress at the central integration point along a radial row of elements. The solid line is equation (4), and the dashed lines are equation (7), referenced either to the inner or outer diameter of the pipe.

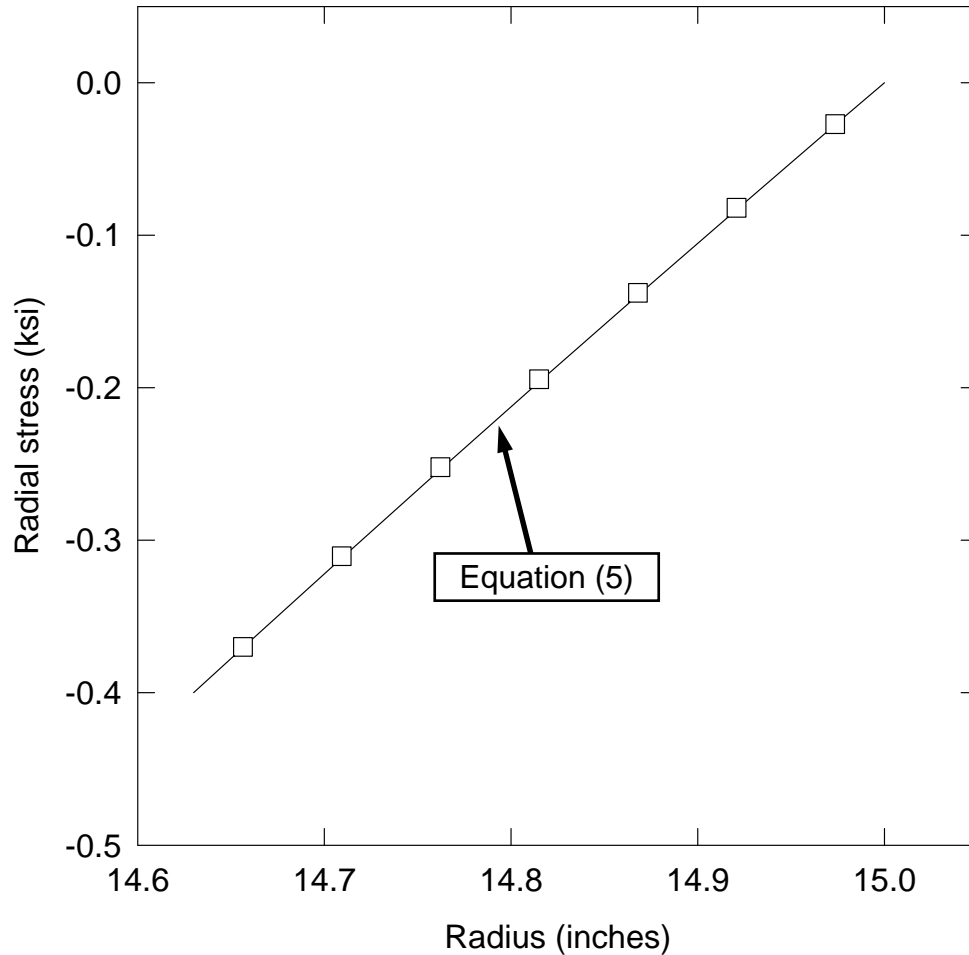


Figure 38. Radial stress in the pipe opposite the weld in Model 2, which has a welded seam with incomplete penetration. The internal pressure is 400 psi. Squares represent the stress at the central integration point along a radial row of elements. The solid line is equation (5). The radial stress is equal in magnitude to the pressure (400 psi or 0.4 ksi, with compressive stresses taken as negative) at the inner surface (a radius of 14.63 inches), and equal to zero at the outer surface (a radius of 15 inches).

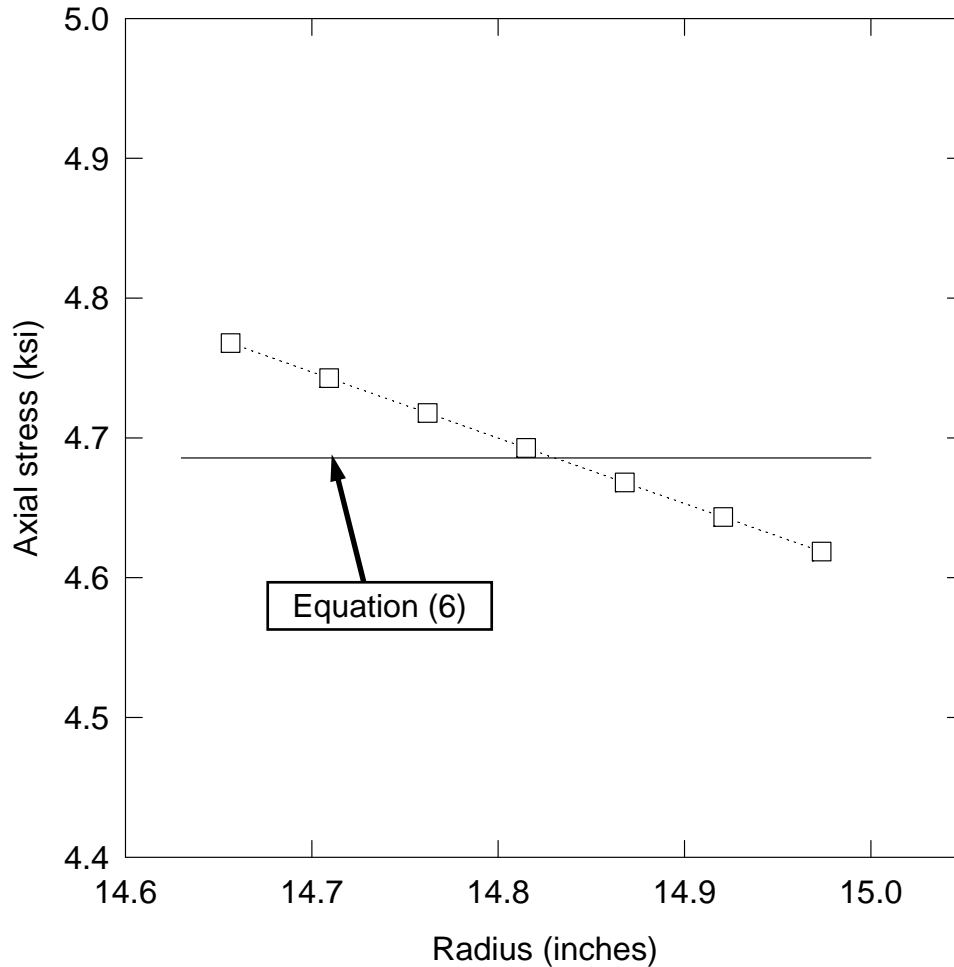


Figure 39. Axial stress in the pipe opposite the weld in Model 2, which has a welded seam with incomplete penetration. The internal pressure is 400 psi. Squares (connected by a dotted line to aid in tracking the data) represent the stress at the central integration point along a radial row of elements. The solid line is equation (6). Because the radial stress is much smaller than the circumferential stress, the axial stress is similar in magnitude to Poisson's ratio times the circumferential stress.